Copy
RM L53J02a

NACA

RESEARCH MEMORANDUM

AERODYNAMIC CHARACTERISTICS IN PITCH OF THREE STRUCTURALLY SIMILAR FLEXIBLE WINGS WITH 45° SWEEP: A SWEPTBACK WING, A WING WITH M PLAN FORM, AND A WING WITH W PLAN FORM

By John W. McKee, Delwin R. Croom, and Rodger L. Naeseth

Langley Aeronautical Laboratory
Langley Field, Va.

NATIONAL ADVISORY COMMITTEE
FOR AERONAUTICS

WASHINGTON

December 14, 1953

NATIONAL ADVISORY COMMITTEE FOR AERONAUTICS

RESEARCH MEMORANDUM

AERODYNAMIC CHARACTERISTICS IN PITCH OF THREE STRUCTURALLY SIMILAR FLEXIBLE WINGS WITH 45° SWEEP: A SWEPTBACK WING, A WING WITH M PLAN FORM, AND A WING WITH W PLAN FORM

By John W. McKee, Delwin R. Croom, and Rodger L. Naeseth

SUMMARY

An investigation has been made in the Langley 300 MPH 7- by 10-foot tunnel to determine the aerodynamic characteristics in pitch of three structurally similar flexible wings with 45° sweep of the quarter-chord line: a sweptback wing, a wing with M plan form, and a wing with W plan form. In addition, a rigid sweptback wing was tested. These semispan wings were tested through a dynamic pressure range from approximately 4.7 to 46 pounds per square foot. The variation of Reynolds number was from approximately 0.4×10^6 to 1.25×10^6. The wings were of aspect ratio 6, taper ratio 0.6, and had NACA 65A009 airfoil sections parallel to the free airstream direction. In addition to the lift, drag, pitching-moment, and bending-moment data, wing deflection and twist angles under airload were measured and some flow surveys were made behind the wings.

The effects of change of plan form from straight sweep to a change of sweep at midsemispan and the large degree of flexibility provided in the models combined to produce some pronounced effects on wing deflection and aerodynamic characteristics.

There was fair agreement between experimentally and theoretically determined twist angles and aerodynamic parameters, with some large differences existing.

INTRODUCTION

The use of thin swept wings in aircraft and missiles being designed for high-speed flight has led to a need for greater knowledge of the

effects of wing flexibility on the wing aerodynamic characteristics. Also, it has been suggested that wings of M or W plan form may possess advantages over straight swept wings. The results of reference 1, which compared the characteristics of the three wings, indicated that the use of an M- or W-plan-form wing rather than a sweptback wing caused significantly different changes in local wing incidence under load than did the swept wing and reduced the irregularity of the pitching-moment variation with lift exhibited at high Mach numbers by the swept wing. The modification of high-aspect-ratio sweptback wings to W plan forms has been found in references 2 and 3 to improve greatly the pitching-moment characteristics at the stall.

Three flexible wings of sweptback and composite (M and W) plan forms and a rigid wing geometrically similar to the flexible sweptback wing were investigated in order to determine the effects of wing flexibility on the aerodynamic characteristics of different plan-form wings and to gain experience in model design and testing technique.

To obtain this information by means of model test is difficult because the model must duplicate the scale geometry and also the scale structural characteristics of the full-scale airplane. Several approaches to the problem of designing a flexible model have been used. Two possible methods are: (1) reproduction of the structure of a prototype airplane by using suitable materials and (2) concentration of the bending and torsional strength in a single beam along a suitable flexural axis, with the profile of the wing being formed by a series of segments attached to the beam in such a manner as not to alter appreciably the stiffness characteristics of the beam. The latter type of model construction, which is by far the cheaper and simpler, was used in the construction of the subject wings.

This paper presents the longitudinal force and moment results and wing deflection and twist angles under airloads for a range of dynamic pressures. In addition, results from theoretical calculations are compared with experimental values, and some downwash data behind the wings are presented.

COEFFICIENTS AND SYMBOLS

C_L lift coefficient, $\dfrac{\text{Twice semispan lift}}{qS}$

C_D drag coefficient, $\dfrac{\text{Twice semispan drag}}{qS}$

C_m pitching-moment coefficient referred to $0.25\bar{c}$, $\dfrac{\text{Twice semispan pitching moment}}{qS\bar{c}}$

C_B bending-moment coefficient about root-chord line, $\frac{\text{Root bending moment}}{q \frac{S}{2} \frac{b}{2}}$

α angle of attack of wing-root chord, deg

q free-stream dynamic pressure, $\rho V^2/2$, lb/sq ft

S twice wing area of semispan model, sq ft

b twice span of semispan model, ft

c local wing chord, ft

$\bar{c}$ mean aerodynamic chord of wing using theoretical tip, $\frac{2}{S}\int_0^{b/2} c^2 dy$, ft

ρ mass density of air, slugs/cu ft

V free-stream velocity, ft/sec

A wing aspect ratio, b^2/S

λ wing taper ratio, ratio of theoretical tip chord to root chord

y lateral distance from plane of symmetry, ft

y_L lateral center of lift, $100 \frac{C_B}{C_L}$, percent semispan

η spanwise station, fraction of semispan, $\frac{y}{b/2}$

θ angle of twist, measured in the free-stream direction, (positive θ trailing edge down), deg

δ vertical deflection of wing spar, upward direction positive, percent semispan

E Young's modulus of elasticity, lb/sq in.

G shear modulus of elasticity, lb/sq in.

I moment of inertia in bending, $in.^4$

J torsional stiffness constant, in.^{4}

C_{L_α} wing lift-curve slope per degree, $\partial C_L/\partial\alpha$

ϵ downwash angle, deg

Subscripts:

R rigid wing

F flexible wing

MODELS

Four models were tested in the present investigation, a rigid and a flexible sweptback wing and flexible wings with an M and W plan form. Throughout the report the models are referred to as the Λ, M, and W wings and the subscripts R and F are used to differentiate between the rigid and flexible sweptback wings. The 3-foot semispan models were of aspect ratio 6, taper ratio of 0.6, and had NACA 65A009 airfoil sections parallel to the free-stream direction (fig. 1). The quarter-chord lines of the wings were swept 45° and the M and W plan forms had sweep breaks at the midsemispan station.

A simple method of construction permitting the design of the flexible models with predetermined structural properties was chosen, that is, a single spar carrying all bending and torsion with the airfoil contour formed by independent segments attached to the spar. The flexible-model structural characteristics were chosen so that the spanwise variation of EI and GJ, EI/GJ ratio, and the torsional axis location were reasonably similiar to airplanes of conventional construction. From comparison of wing structural data for existing airplanes and characteristics of various cross sections, it was found that a round steel spar (with $E = 29 \times 10^6$ psi and $G = 11.6 \times 10^6$ psi) had a reasonably representative EI/GJ ratio (1.25), and that placing the spar on the 0.40 chord line was a reasonable choice.

Typical construction of the flexible models is shown in figures 2 and 3. The balsa segments forming the wing contours were attached to the spar by steel rods through the center of the balsa. The slots between the segments and the clearance space around the spar were filled with grease. The wing was stiffened in the chordwise direction by means of rubber blocks glued to only one of any two adjacent balsa segments at the leading and trailing edges of the wing. (See detail of fig. 2.) When thoroughly greased, this stiffening had a very small effect on vertical

bending and torsional characteristics of the wings for the angle-of-attack range investigated.

A rigid sweptback wing of the same geometry as the flexible sweptback wing was constructed of mahogany wood reinforced with steel.

The spanwise variation of EI of the flexible sweptback wing model was derived from the assumption of a stressed-skin duralumin wing designed to carry a load distributed spanwise in proportion to the local chord with a constant spanwise bending stress. A wing-bending stress of 40,000 pounds per square inch in the wing outermost fiber was simulated for the condition of a model wing loading $(C_L q)$ of 8 pounds per square foot. The required variation of the radius of a round steel spar for the model was calculated from these assumptions and is shown in figure 4; it can be seen that a spar with a straight taper ratio of 0.3 very nearly duplicates the theoretical spar and use of this straight taper spar was decided upon for ease of machining.

Two wings, geometrically, aerodynamically, and structurally similar, but of different scale, will have a similar deflected shape due to airload when the factor EI/qb^4 is the same for both wings. For purposes of comparison, an EI curve for the Boeing B-47 airplane wing scaled down by a q ratio of 87.7 to 8 and a span ratio of 116 to 6 is shown in figure 5. The Boeing B-47 wing is not geometrically the same as the model (aspect ratio 9.43, leading edge swept back 36.6°, taper ratio 0.42, and NACA 65012 airfoil section parallel to the free airstream direction) and certainly was not designed by the simplified assumptions used in the model design. However, a general resemblance is seen in the curves, the Boeing B-47 wing being stiffer at the tip and more flexible at the root than the model spar.

The sweptback segments of spar for the M- and W-plan-form wings have the same dimensions as the corresponding spar lengths for the sweptback wings. The sweptforward spar segments for the M- and W-plan-form wings were based on calculations for a sweptforward wing spar by using the same conditions as for the sweptback wing spar. Because the spar does not coincide with the quarter-chord line, the sweptforward spar is slightly longer than the sweptback spar; therefore, slightly greater computed EI values resulted. The variation of EI and GJ with spanwise stations for the spars of three flexible wings determined experimentally by measuring deflections from applied loads is given in figure 6. The differences in the curves are due to the slightly different lengths of the spars in the sweptforward parts as compared with the respective sweptback parts and the difficulty of machining the spars to the very small tolerance required for negligible change in I. The values of EI were found to vary up to 8 percent from the calculated values of EI based on $E = 29 \times 10^6$ pounds per square inch. The measured EI/GJ ratio averaged

close to the expected value of 1.25. The discontinuities in the EI and GJ curves of the M- and W-plan-form wings from $\eta = 0.48$ to 0.52 are at spar junctures where a steel block of width $0.04b/2$ was used to join the spar parts.

APPARATUS

The investigation was made in the Langley 300-MPH 7- by 10-foot tunnel. In order to test the semispan models in a region outside the tunnel boundary layer, a reflection plane was mounted about 3 inches from the tunnel wall as shown in figure 3. The reflection-plane boundary-layer thickness was such that a value of 95 percent of the free-stream dynamic pressure was reached at a distance of 1.7 inches from the surface at the balance center line for all test dynamic pressures. This thickness represents a distance of 4.7 percent semispan for the models tested. A 1/8-inch-thick metal end plate was attached to the root of the models to cover the slot cut in the reflection plane for the wing butt (fig. 3). Data were obtained by using a strain-gage balance system mounted outside the tunnel. In addition to the force and moment measurements, bending and torsional deflections of the wing were measured. These data were obtained by using a cathetometer mounted outside of the test section to measure the vertical deflections of targets attached to the leading and trailing edges of the wing at several spanwise stations as shown in figure 3(b). The balance was replaced by a rigid mounting assembly for these deflection tests. Force and moment measurements were made with targets off.

TESTS

Tests were performed at dynamic pressures approximately from 4.7 to 46 pounds per square foot. Reynolds numbers based on the mean aerodynamic chord of the models varied approximately from 0.4×10^6 to 1.25×10^6. Angles of attack and dynamic pressures were limited to the values shown in the results by the maximum design lift of 24 pounds, the tendency of the Λ_F wing and the M wing to flutter, and by the unsteady behavior (tendency toward diverging) of the W wing. Flexible-wing deflections and twist angles were obtained from tests at representative angles of attack and several dynamic pressures. Flow surveys were made with a yaw head in a plane $1.22b/2$ behind the Λ_R wing, the Λ_F wing, and the M wing. The W wing was lost during the force testing when the outboard wing panel diverged.

CORRECTIONS

Jet-boundary corrections, determined by the method presented in reference 4, have been applied to the angle of attack. Blockage corrections are negligible; hence, they have not been made in the present tests. No correction has been applied to the drag coefficient to account for the effect of the end plate at the root of the model.

RESULTS AND DISCUSSION

Presentation of Results

Results of the investigation are presented in the following figures:

	Figures
Basic aerodynamic data	7 to 10
Bending deflection data	11
Wing-twist data	12
Comparison of wing deflection, wing twist, and spar twist for C_Lq of 4	13
Comparison of theoretical and measured twist angles	14
Summary of aerodynamic characteristics	15
α against C_L for constant C_Lq	16
C_m against C_L for constant C_Lq	17
Downwash data	18

Deflection Characteristics

The vertical deflections of the Λ_F-, M-, and W-plan-form wings under airloads are similar in shape but differ in magnitude (figs. 11 and 13); the wing-twist angles are quite dissimilar (figs. 12 and 13). The wing-twist angles result from the combination of the streamwise components of spar bending and spar twist. Bending due to upward airloads of a sweptback wing results in a decrease in local angle of attack relative to the wing root, whereas bending due to upward airloads of a sweptforward wing results in an increase in local angle of attack relative to the wing root. Torsional span twist in a plane normal to the elastic axis is such that, when it is referred to the streamwise direction, it produces an increase in local angle of attack relative to the wing root for both sweptback and sweptforward wings. This change in local angle of attack due to torsion for the Λ_F wing (fig. 13) is about 24 percent of the change due to bending for $\eta = 1.0$ and about 12 percent for $\eta = 0.5$. These data are in good agreement with the values calculated in reference 5 for thin, highly swept wings.

Changing a swept wing to an M- or W-plan-form wing will cause the loading outboard of the sweep break to apply a large torsional moment and a reduced bending moment to the inboard section of the wing. These changes of moments can be such, if the change of sweep is correctly made by taking into account among other things the wing spanwise stiffness characteristics, as to reduce the magnitude of the streamwise twist of M- or W-plan-form wings below that of the swept wing and greatly reduce the variation of aerodynamic parameters with dynamic pressure. It can be seen in figure 13 that the Λ_F wing had negative twist, increasing from root to tip but more slowly at the tip (as previously mentioned the predominant factor producing streamwise twist was wing bending), the M wing had greatly reduced twist which was positive inboard and negative outboard of about the 0.65b/2 station, and the W wing had essentially zero twist over the inboard 0.3b/2 and positive twist increasing rapidly to the tip.

Lift Characteristics

A comparison of the variation of C_{L_α} (measured near zero lift) with dynamic pressure for the Λ wings indicated a constant C_{L_α} of 0.0607 for the Λ_R wing and a decrease in C_{L_α} for the Λ_F wing with increase in dynamic pressure (fig. 15). The decrease in the lift-curve slope of the flexible wing is a natural consequence of the increase of negative twist with dynamic pressure shown in figure 12.

The M- and W-wing results (fig. 15) indicate an increase in C_{L_α} with an increase in dynamic pressure, the rate of increase being much less for the M wing. The twist angles, as shown in figure 12, indicate a net increase in angle of attack for the M and W wings; however, a greater net increase was noted for the W wing.

The basic data were cross-plotted to determine the variation of angle of attack with lift coefficient at several constant wing loadings (in this form the data are applicable to a level-flight condition) (fig. 16). The $C_L q = 0$ curves were obtained from the Λ_R-wing data for the Λ_F wing and were obtained by extrapolating to $q = 0$ for the M and W wings. The Λ_F-wing lift-curve slope decreased some with wing loading and the lift curves were displaced to larger angles of attack for constant lift coefficient as the wing loading was increased (in effect equivalent to an increase of flexibility at constant wing loading). The M wing had a lift curve that was little affected by wing loading, the curves at various wing loadings being very nearly equal to the curve that would be obtained for a rigid wing. The lift curves of the W wing seem somewhat more erratic than the Λ_F and M wings partially because above $C_L = 0.5$ the wing stall commences. The lift-curve slope was decreased some by wing

loading and the angle of attack for a given lift coefficient was reduced as the wing loading was increased.

The variations of lateral center of lift with increasing dynamic pressure for the wings (fig. 15) are an inboard movement for the Λ_F wing, a slight inboard movement for the M wing, and a large outboard movement for the W wing. An examination of the spanwise variation of angles of twist (fig. 12) indicates that these movements of lateral center of lift are no doubt caused by the shift in span loadings resulting from the reduction in angle of attack from root to tip on the Λ_F wing, the combination of an increase in angle of attack of the inboard and a decrease in angle of attack of the outboard parts of the M wing, and a large increase in angle of attack over the outboard part of the W wing with increase of dynamic pressure.

Pitching-Moment Characteristics

Throughout the test dynamic-pressure range, near zero lift, aerodynamic-center locations of approximately 24, 22.5, and 31 percent mean aerodynamic chord were measured for the Λ_R, M, and W wings, respectively; however, the aerodynamic center of the Λ_F wing shifted forward with an increase in dynamic pressure (fig. 15). The variation of pitching-moment coefficient with lift coefficient for all wings (fig. 9) was linear up to a lift coefficient of approximately 0.45. Near a lift coefficient of 0.5, the Λ_R wing had an abrupt unstable break in the pitching-moment curve, whereas the break was more gradual for the Λ_F wing. The curves for the M and W wings did not exhibit this large change of pitching-moment slope at the higher lift coefficients.

The pitching-moment data were cross-plotted to determine the variation of pitching-moment coefficient with lift coefficient at several constant wing loadings (fig. 17). The constant-wing-loading curves indicated an increase in pitching-moment coefficient with increase of wing loading at a constant lift coefficient for the Λ_F wing; no appreciable change in pitching-moment coefficient at a given lift coefficient was observed for the M or W wings. The aerodynamic center of the Λ_F wing was essentially unaffected by wing loading for loadings of 2, 4, and 6 pounds per square foot and was the same as the aerodynamic center for the rigid-wing or zero-dynamic-pressure case below $C_L = 0.3$. The aerodynamic-center locations of the M and W wings were about constant and the same for the case of constant wing loading as those obtained for constant dynamic pressure.

Drag Characteristics

The minimum drag coefficient for the wings was essentially the same and showed negligible change with dynamic pressure. (End-plate drag is included in these results (fig. 8).) An increase in drag coefficient due to lift coefficient was anticipated for the flexible wings because of the discontinuities in the surface when the wings deflect under airloads; however, an examination of the results indicates that the Λ_F wing drag due to lift was lower than for the Λ_R wing. It appears that the decrease in angle of attack from root to tip has a beneficial effect on the flow over the wing and that the discontinuities in the surface have little effect on the drag.

The drag for the M wing, at the higher lift coefficients, was slightly lower than for the Λ wings; this effect is mainly attributed to flow improvement resulting from change of plan form rather than from benefical twist. The W-wing results indicated a more rapid rise of drag due to lift at moderate lift coefficients. Results of a previous investigation of a rigid W wing (ref. 6) indicated that an increase in drag is caused by separation at the juncture. However, the drag at high lift coefficients is far greater than that obtained in reference 6, and the stall occurred at a lower lift coefficient. These differences are likely caused by the increase in angle of attack of the outboard panel of the flexible wing and the lower Reynolds number resulting in an earlier stall.

Downwash

The downwash data (fig. 18) were obtained at five spanwise stations and at five vertical stations in one plane behind the wing; therefore, not enough data were obtained to establish completely the flow field behind the wing. These data are presented without discussion.

Theory

Description of theoretical method.- Reference 7 presents a method whereby the wing twist angles of a swept flexible wing can be determined for approximately equilibrium conditions. Since M- and W-plan-form wings can be thought of structurally as a sweptforward wing and a sweptback wing, the method outlined in reference 7 lends itself readily to computing twist angles of these plan forms. The span load distribution of the rigid wings associated with angle of attack (referred to as the additional loading) was obtained from reference 8, and the span load distribution of the rigid wing associated with twist (referred to as the basic loading) was obtained for the sweptback wing from reference 9, and for the M and W wings by the method of reference 8.

When the theoretical twist angles were determined, the additional loading was applied along the quarter-chord line and the twist due to this load was determined. Then, the basic loading was applied and the resulting twist due to basic loading was obtained. From these two types of twist, the factor K of reference 7 (ratio of twist due to basic loading to twist due to additional loading) was determined. It should be noted, however, that the basic loadings given in reference 9 are for a linear twist; therefore, the twist as obtained from the additional loading was approximated by a straight line for the Λ_F wing in these calculations. Since the twist of M- and W-plan-form wings cannot be approximated as a straight line, the actual twist distribution obtained from the additional loading of the M- and W-plan-form wings was used to determine the basic loadings of the M and W wings by the method of reference 8. Tabular integration (outlined in ref. 7) and mechanical integration of the bending and torsional moment diagrams yielded the same results for the Λ_F wing. Mechanical integration was used to obtain areas of the bending- and torsional-moment diagram of the M and W wings.

The K factor as used in reference 7 was determined for the Λ_F wing as that value at the tip, and for the sweptback and sweptforward parts of the composite plan form as that value at the midsemispan and at the tip. The sweptback and sweptforward parts of the M and W wings were treated separately in these calculations, the resulting twist angles being obtained by the principal of superposition.

The calculated variation of y_L, dC_m/dC_L, and C_{L_α} with dynamic pressure is presented in figure 15. The lateral center of lift was obtained by integrating the aeroelastic span loadings. The assumption was made that the loading was along the quarter chord; therefore, by geometry (ref. 8 gives this relation for M and W wings) the aerodynamic-center location was obtained. The lift-curve slope for the three wings was obtained by the method outlined in reference 7.

Comparison of experiment and theory.- Aeroelastic effects were calculated by the theory of reference 7. A comparison of the calculated and experimental wing twist angles is presented in figure 14 and a comparison of calculated and experimental aerodynamic characteristics is presented in figure 15. Some large discrepancies are shown between the experimentally and theoretically determined twist angles and aerodynamic characteristics, but, in general, there is fair agreement in their variation with dynamic pressure. The theory of reference 7 is limited to small deflections because it is based on simple beam theory. Comparison of radii of curvature calculated from the experimental deflection curves by using exact and simple beam theory indicated that a substantial part of the error at the higher C_Lq values results from violation of a basic assumption of simple beam theory that the bending deflections be small.

CONCLUDING REMARKS

An investigation has been made in the Langley 300 MPH 7- by 10-foot tunnel to determine the aerodynamic characteristics in pitch of three structurally similar flexible wings with 45° sweep of the quarter-chord line: a sweptback wing, a wing with M plan form, and a wing with W plan form. The effects of change of plan form from straight sweep to a change of sweep at midsemispan and the large degree of flexibility provided in the models combine to produce some pronounced effects on wing deflection and aerodynamic characteristics. The following effects were particularly noticeable:

1. Wing twist angles measured in the streamwise direction for the swept wing were negative and became larger from root to tip; for the M-plan-form wing, the angles averaged slightly positive with small negative values at the tip; and, for the W plan-form wing, the angles were small over the inboard section with a rapid positive increase over the outboard section. The magnitude of the twist angles increased with lift coefficient and dynamic pressure.

2. The effect of wing twist was apparent in the variation of aerodynamic parameters with increase of dynamic pressure: the lift-curve slope decreased, the aerodynamic center moved forward, and the lateral center of lift moved inboard for the swept wing; the lift-curve slope increased rapidly and the lateral center of lift moved outboard for the W-plan-form wing; and the parameters of the M-plan-form wing were affected to a lesser extent.

3. The swept rigid wing had a pronounced unstable break in the pitching-moment curve at a lift coefficient of 0.5 whereas the swept flexible wing had a more gradual unstable break in the pitching-moment curves. The M- and W-plan-form wings had pitching-moment slopes that were much more nearly linear up to the stall and the position of the aerocynamic center was practically unaffected by dynamic pressure.

4. The drag due to lift of the swept flexible wing was lower than that of the rigid wing, presumably because of favorable twist effects. The drag of the M-plan-form wing at high lift coefficient was lower than that of the swept wing; this effect is mainly attributed to flow improvement resulting from change of plan form rather than twist. The W-plan-form wing had a more rapid rise of drag with lift coefficient which was attributed to unfavorable plan-form effect and increased angle of attack of the outboard section of the wing leading to tip stall.

5. There was fair agreement between experimentally and theoretically determined twist angles and aerodynamic parameters, with some large differences existing.

6. When the data were examined on the basis of constant wing loading (applicable to a level-flight condition) rather than constant dynamic pressure (maneuvers) it was found that the lift-curve slope decreased some and the lift curves were displaced to larger angles of attack for constant lift coefficient with increase of wing loading (in effect equivalent to an increase of flexibility at constant wing loading) for the swept wing, the lift characteristics were little affected for the M-plan-form wing, and the lift-curve slope decreased some and the angle of attack for a given lift coefficient was reduced with increase of wing loading for the W-plan-form wing. The aerodynamic center of the swept wing was essentially unaffected by wing loading for loadings of 2, 4, and 6 pounds per square foot and was the same as the aerodynamic center for the rigid wing or zero dynamic pressure case below a lift coefficient of 0.3. The aerodynamic-dynamic-center locations of the M- and W-plan-form wings were about constant and the same as for the constant-dynamic-pressure cases.

Langley Aeronautical Laboratory,
National Advisory Committee for Aeronautics,
Langley Field, Va., September 28, 1953.

REFERENCES

1. Campbell, George S., and Morrison, William D., Jr.: A Small-Scale Investigation of "M" and "W" Wings at Transonic Speeds. NACA RM L50H25a, 1950.

2. Morrison, William D., Jr.: Transonic Aerodynamic Characteristics of Three W-Plan-Form Wings Having Aspect Ratio 8, Taper Ratio 0.45, and NACA 63A-Series Airfoil Sections. NACA RM L52E14a, 1952.

3. Purser, Paul E., and Spearman, M. Leroy: Wind-Tunnel Tests at Low Speed of Swept and Yawed Wings Having Various Plan Forms. NACA TN 2445, 1951. (Supersedes NACA RM L7D23.)

4. Polhamus, Edward C.: Jet-Boundary-Induced-Upwash Velocities for Swept Reflection-Plane Models Mounted Vertically in 7- by 10-Foot, Closed, Rectangular Wind Tunnels. NACA TN 1752, 1948.

5. Frick, C. W., and Chubb, R. S.: The Longitudinal Stability of Elastic Swept Wings at Supersonic Speed. NACA Rep. 965, 1950. (Supersedes NACA TN 1811.)

6. Polhamus, Edward C., and Becht, Robert E.: Low-Speed Stability Characteristics of a Complete Model With a Wing of W Plan Form. NACA RM L52A25, 1952.

7. Skoog, Richard B., and Brown, Harvey H.: A Method for the Determination of the Spanwise Load Distribution of a Flexible Swept Wing at Subsonic Speeds. NACA TN 2222, 1951.

8. Campbell, George S.: A Finite-Step Method for the Calculation of Span Loadings of Unusual Plan Forms. NACA RM L50L13, 1951.

9. DeYoung, John, and Harper, Charles W.: Theoretical Symmetric Span Loading at Subsonic Speeds for Wings Having Arbitrary Plan Form. NACA Rep. 921, 1948.

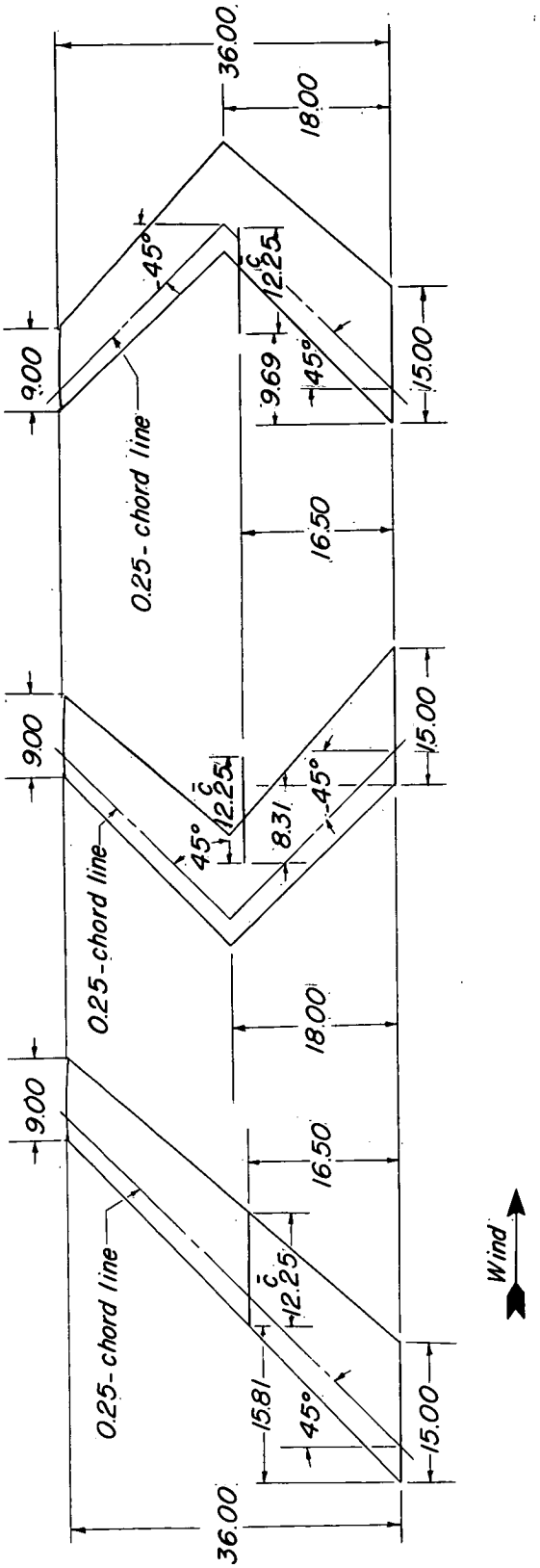

Tabulated Wing Data, Λ Wing	
Sweep	45°
Aspect ratio	6
Taper ratio	0.6
Airfoil section parallel to free stream	NACA 65A009
Area (twice semispan)	6.00 sq ft

Tabulated Wing Data, M Wing	
Sweep of inboard panel	-45°
Sweep of outboard panel	45°
Aspect ratio	6
Taper ratio	0.6
Airfoil section parallel to free stream	NACA 65A009
Area (twice semispan)	6.00 sq ft

Tabulated Wing Data, W Wing	
Sweep of inboard panel	45°
Sweep of outboard panel	-45°
Aspect ratio	6
Taper ratio	0.6
Airfoil section parallel to free stream	NACA 65A009
Area (twice semispan)	6.00 sq ft

Figure 1.- Plan-form drawing of the Λ, M, and W wings. All dimensions are in inches unless otherwise noted.

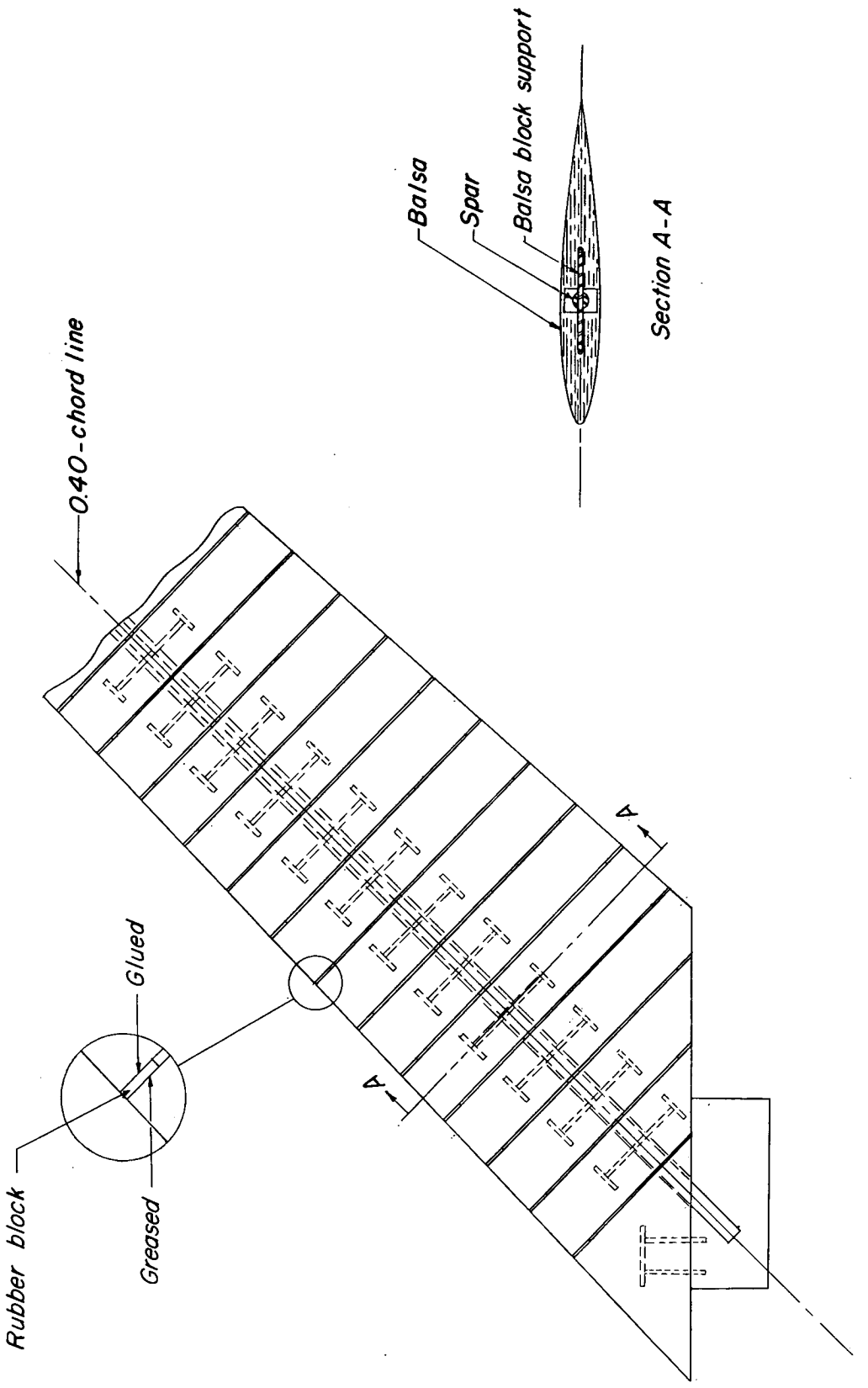

Figure 2.- Typical construction of the flexible wing models.

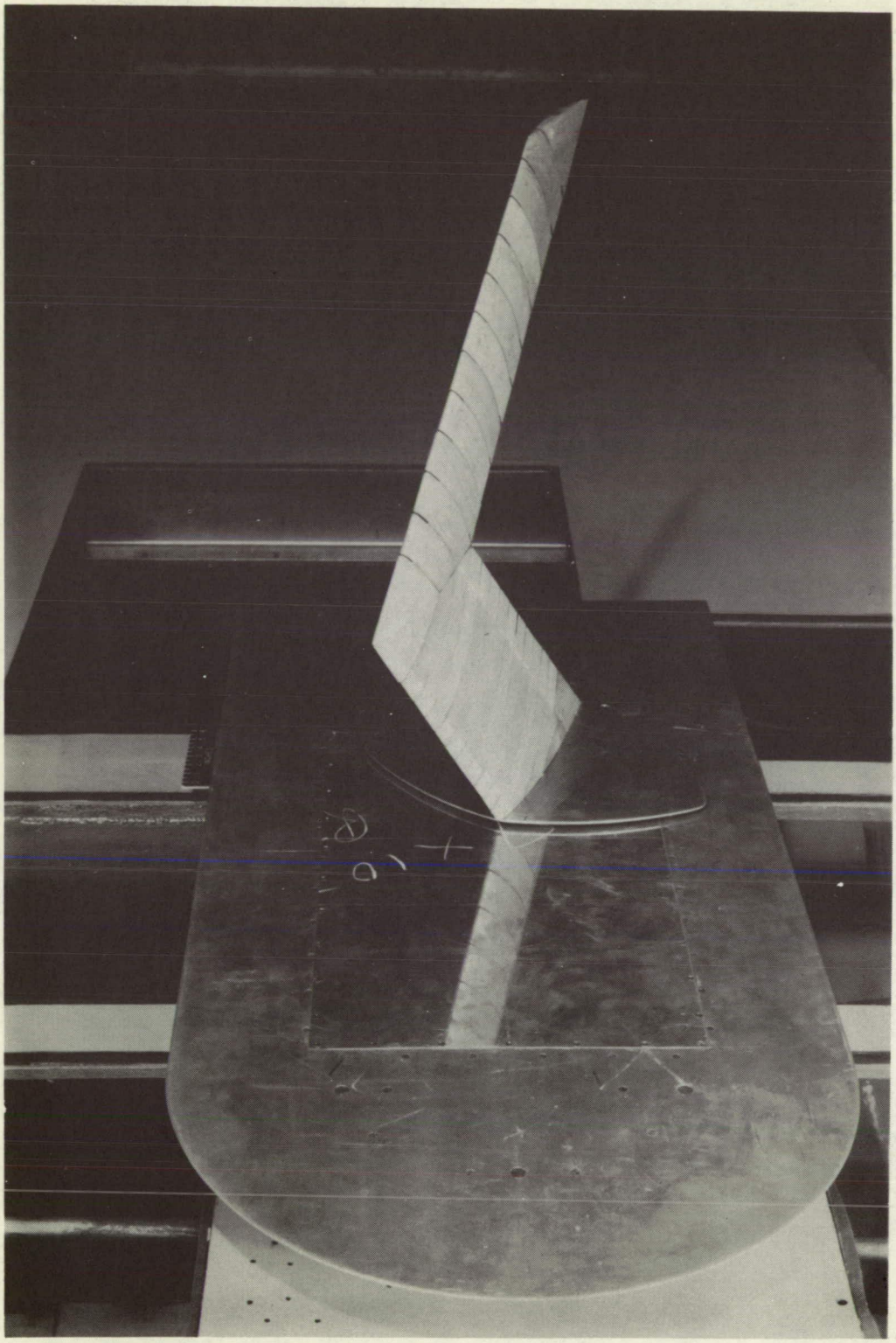

L-68735

(a) M-plan-form wing.

Figure 3.- Reflection plane model in the Langley 300 MPH 7- by 10-foot tunnel.

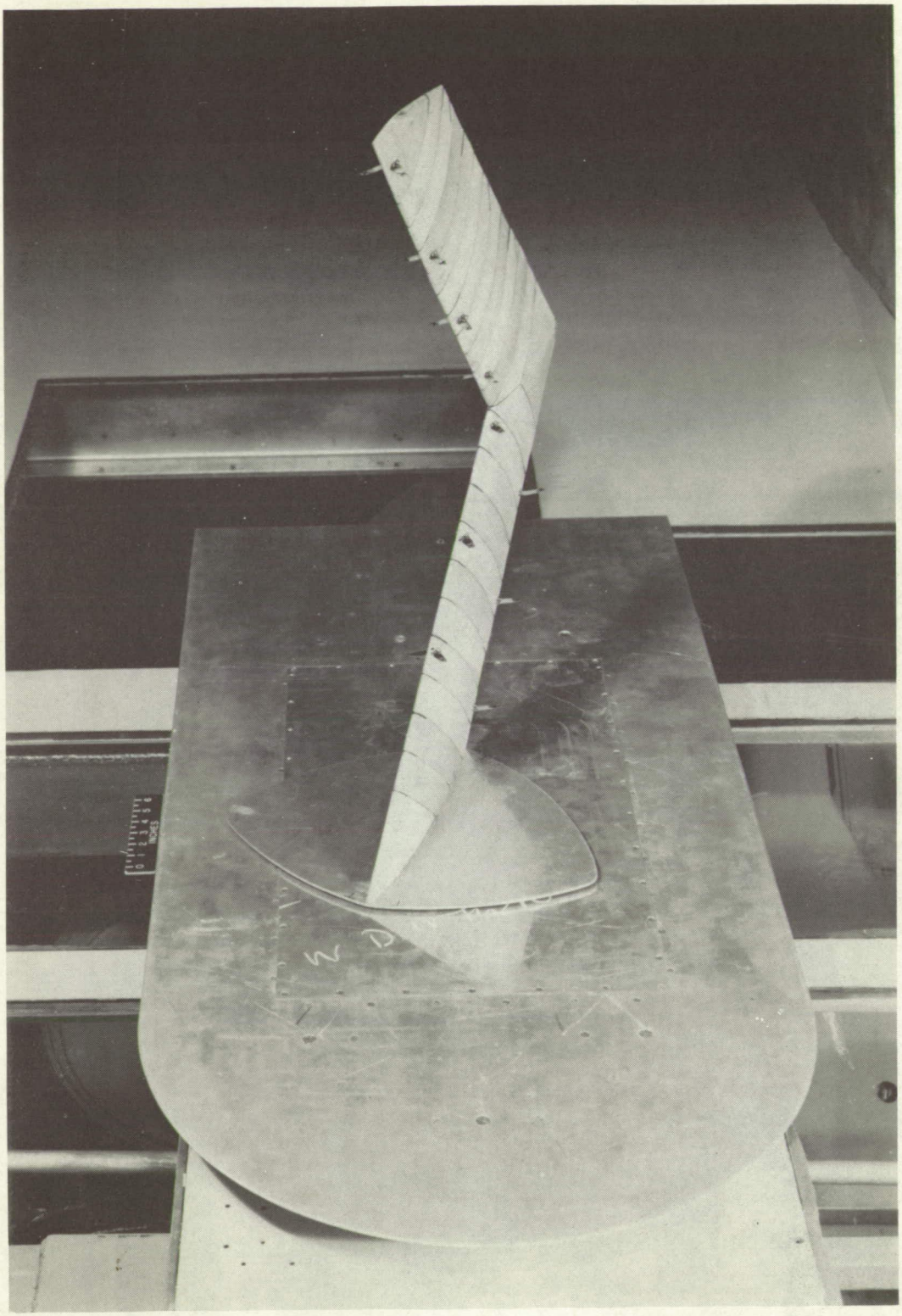

L-68731

(b) W-plan-form wing with targets.

Figure 3.- Concluded.

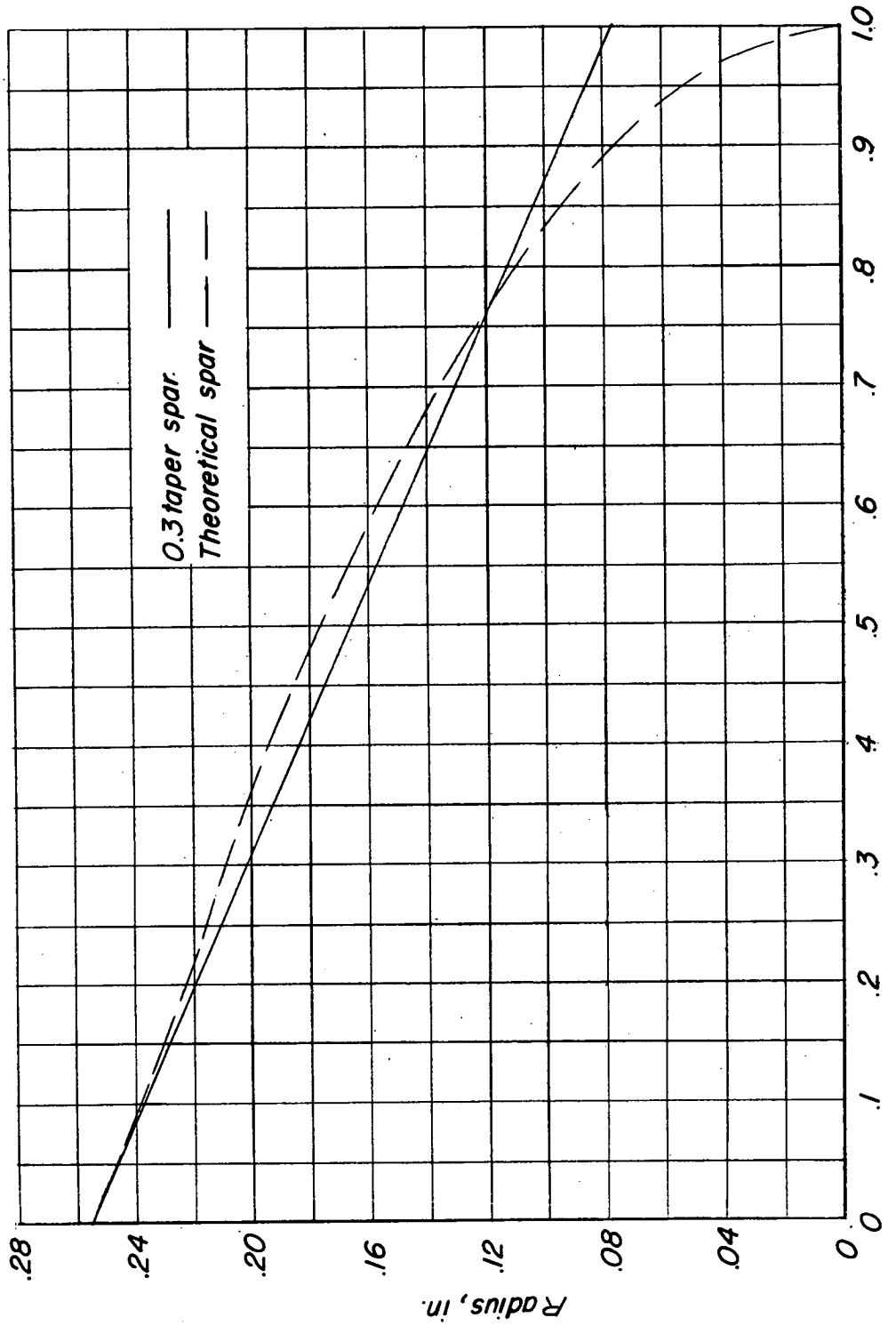

Figure 4.- Variation of radius of spars for the swept back wing with spanwise positions (sections normal to the axis of the spar).

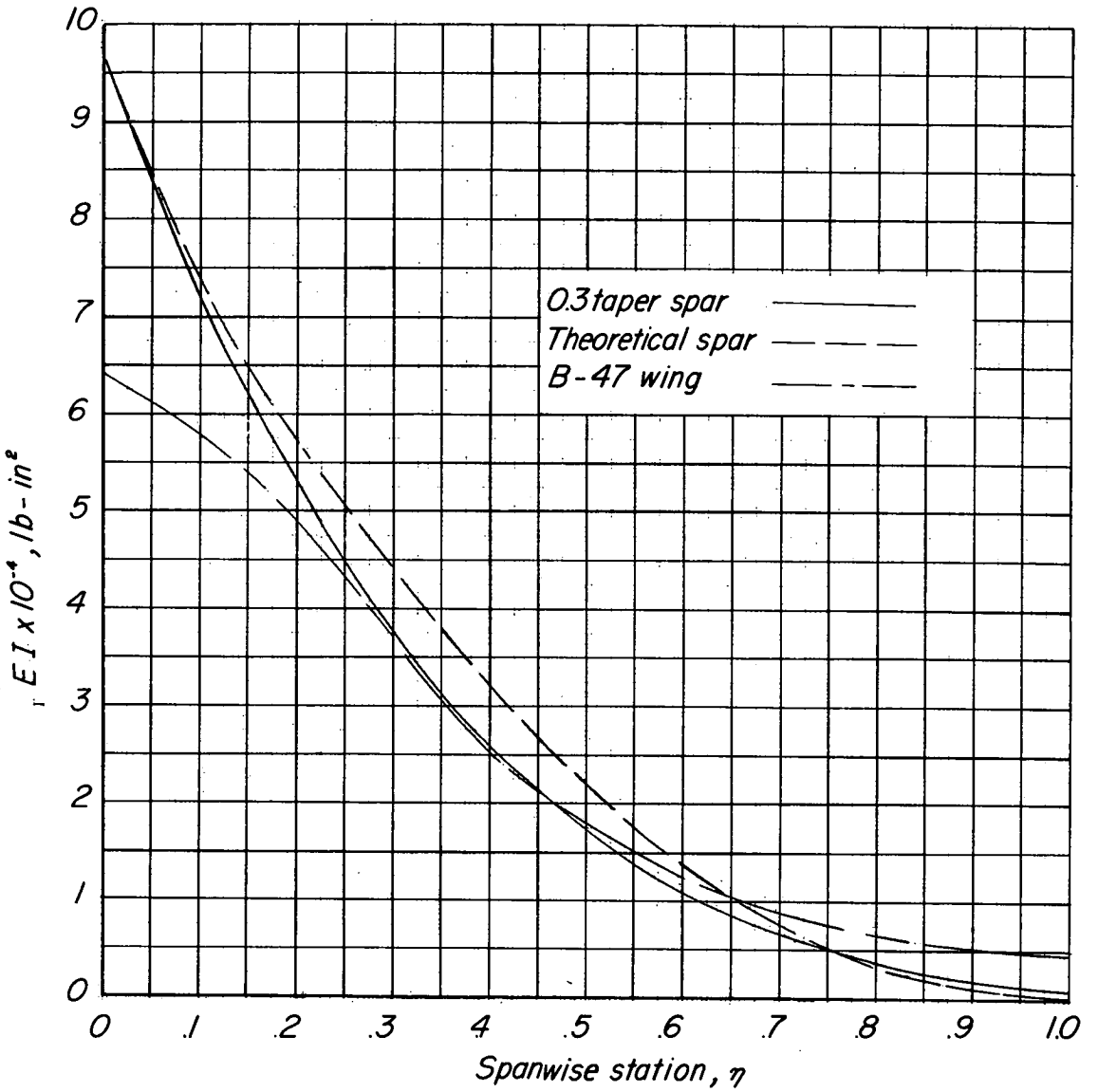

Figure 5.- Spanwise variation of bending rigidity of the 0.3 taper spar as designed, the theoretical spar as designed, and the Boeing B-47 wing scaled by a q ratio of 87.7 to 8 and a span ratio of 116 to 6 (sections normal to elastic axis).

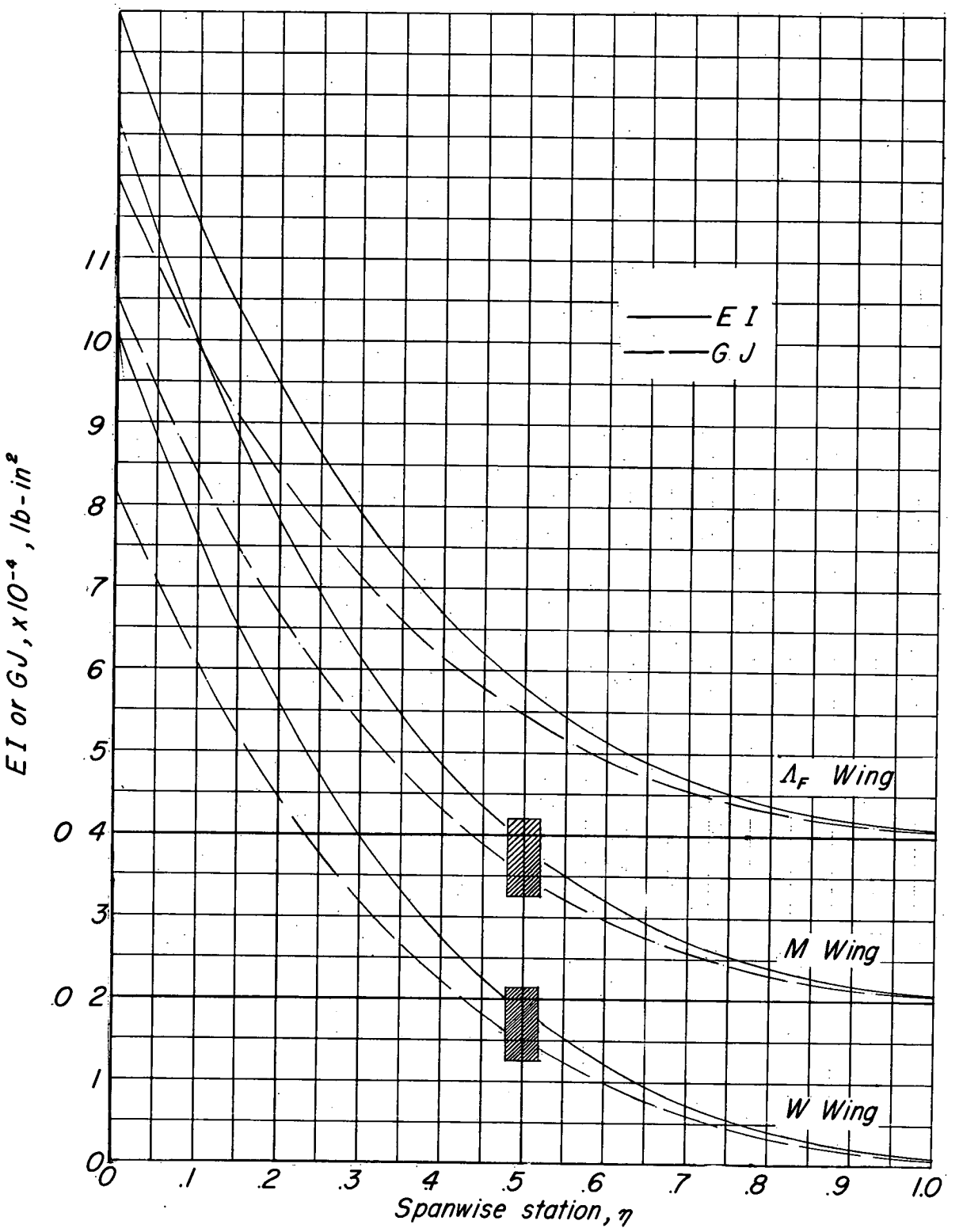

Figure 6.- Measured spanwise variation of bending and torsional rigidity for Λ, M, and W wings. (Sections normal to the axis of the spar.)

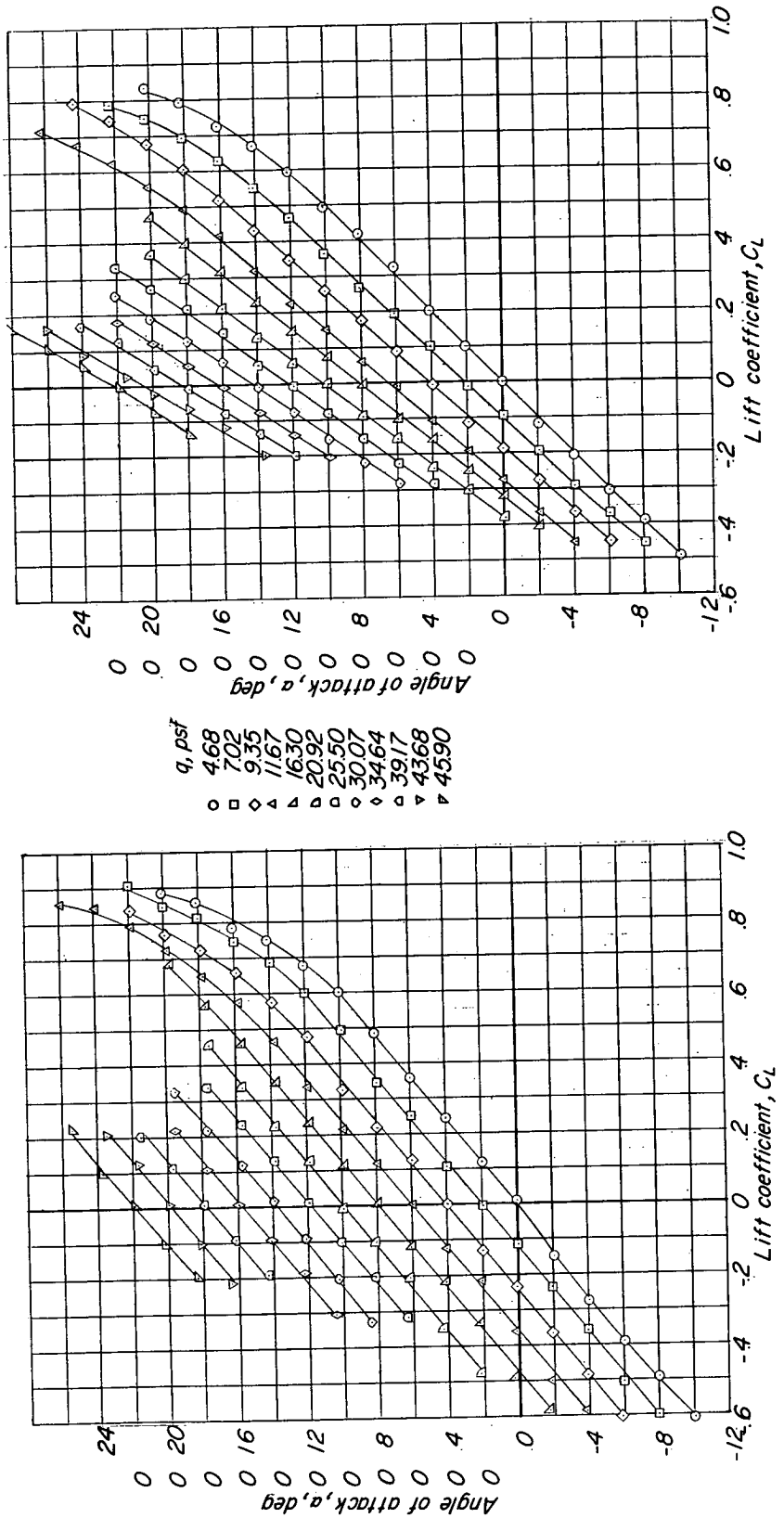

(a) Λ_R wing.

(b) Λ_F wing.

Figure 7.- Variation of angle of attack with lift coefficient for various dynamic pressures.

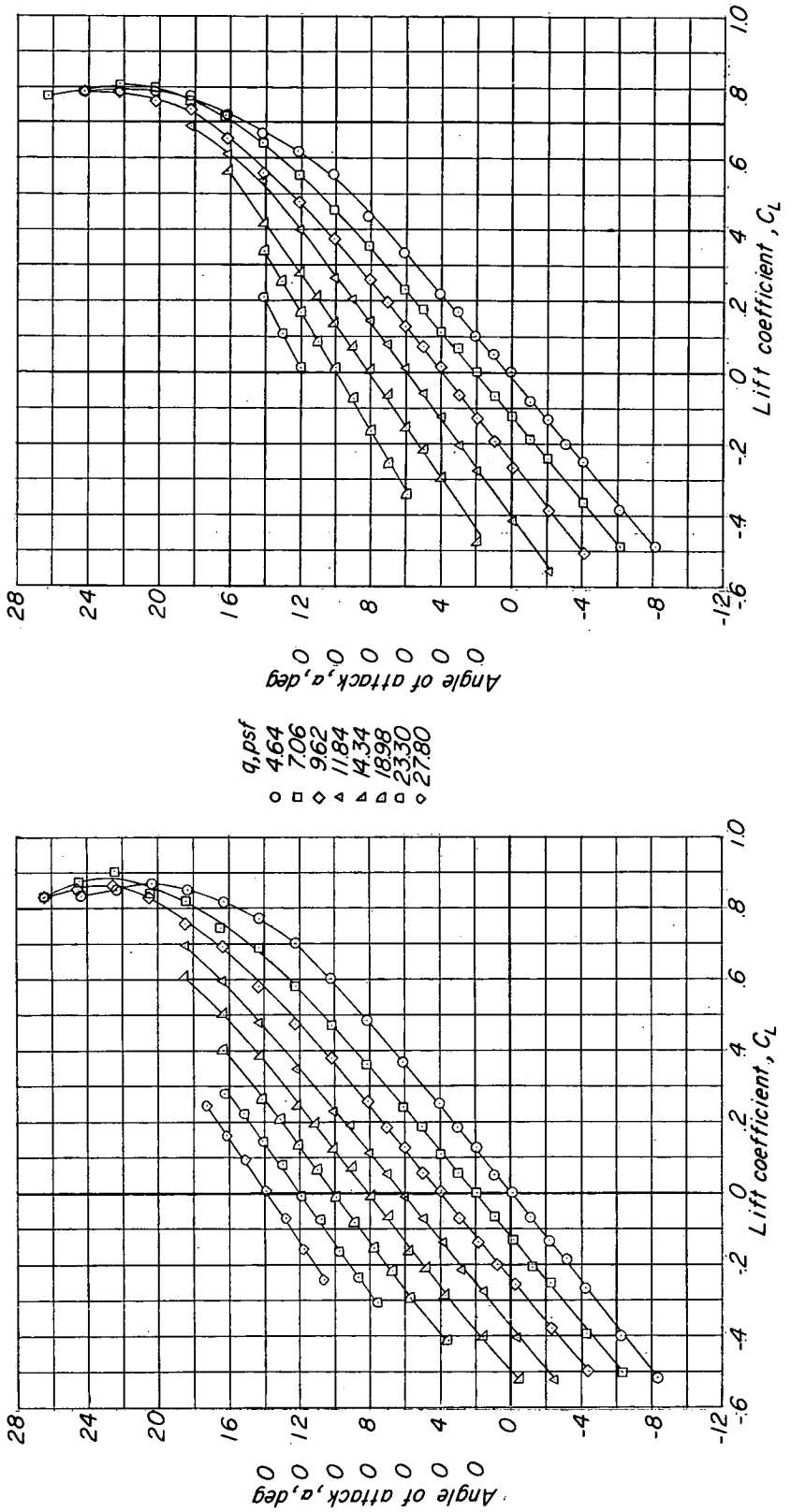

(c) M wing.

(d) W wing.

Figure 7.- Concluded.

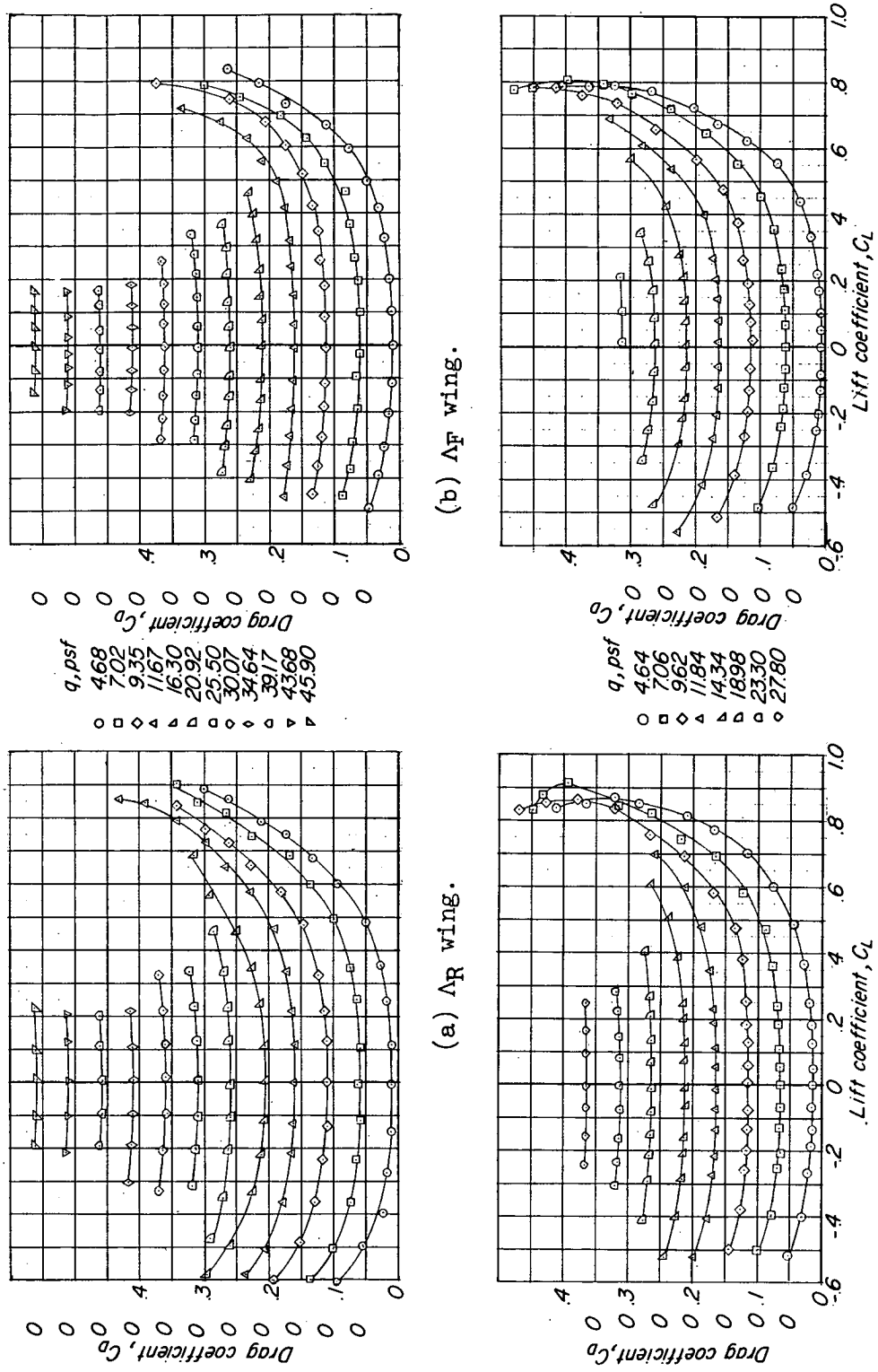

Figure 8.- Variation of drag coefficient with lift coefficient for various dynamic pressures.

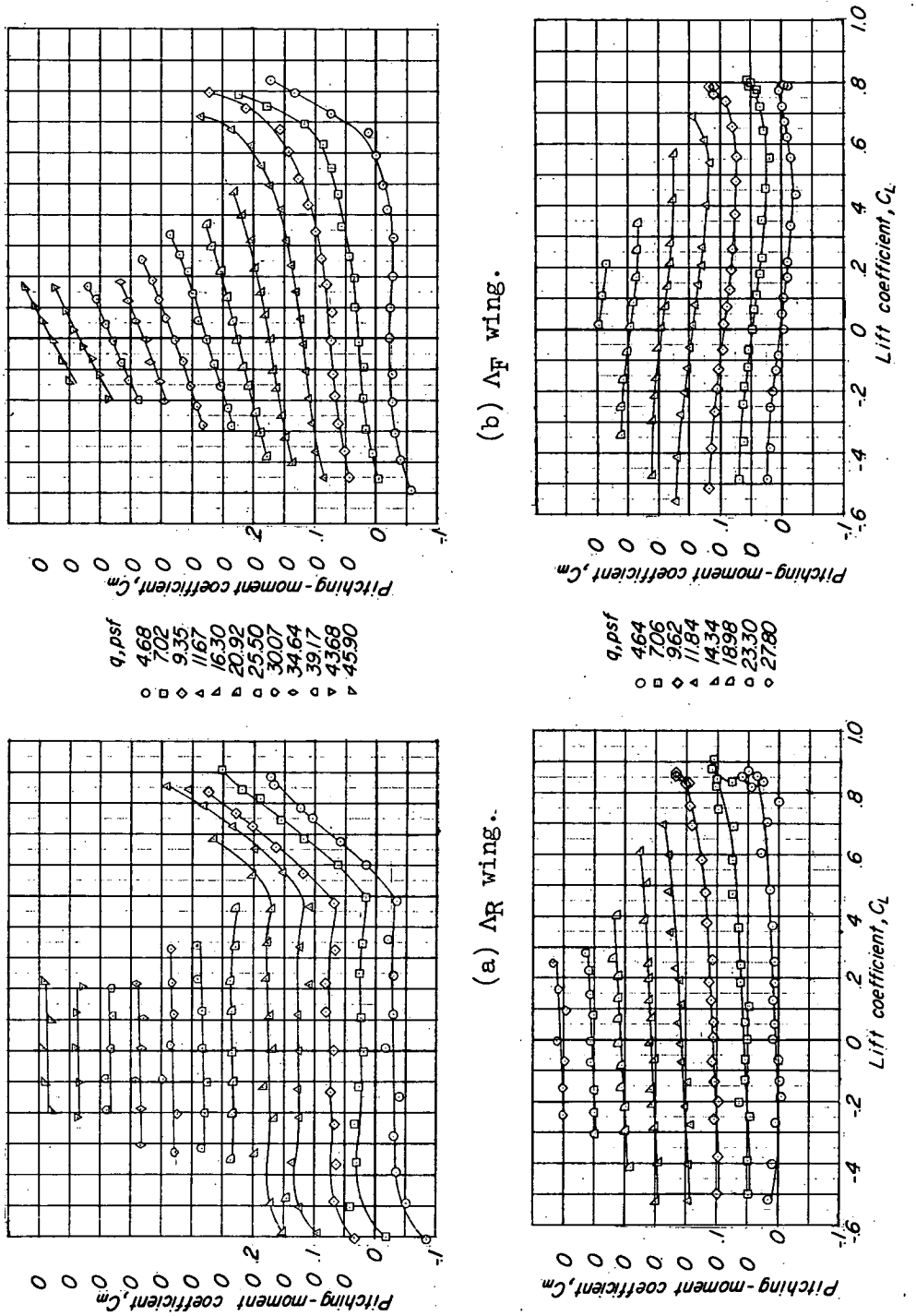

Figure 9.- Variation of pitching-moment coefficient with lift coefficient for various dynamic pressures.

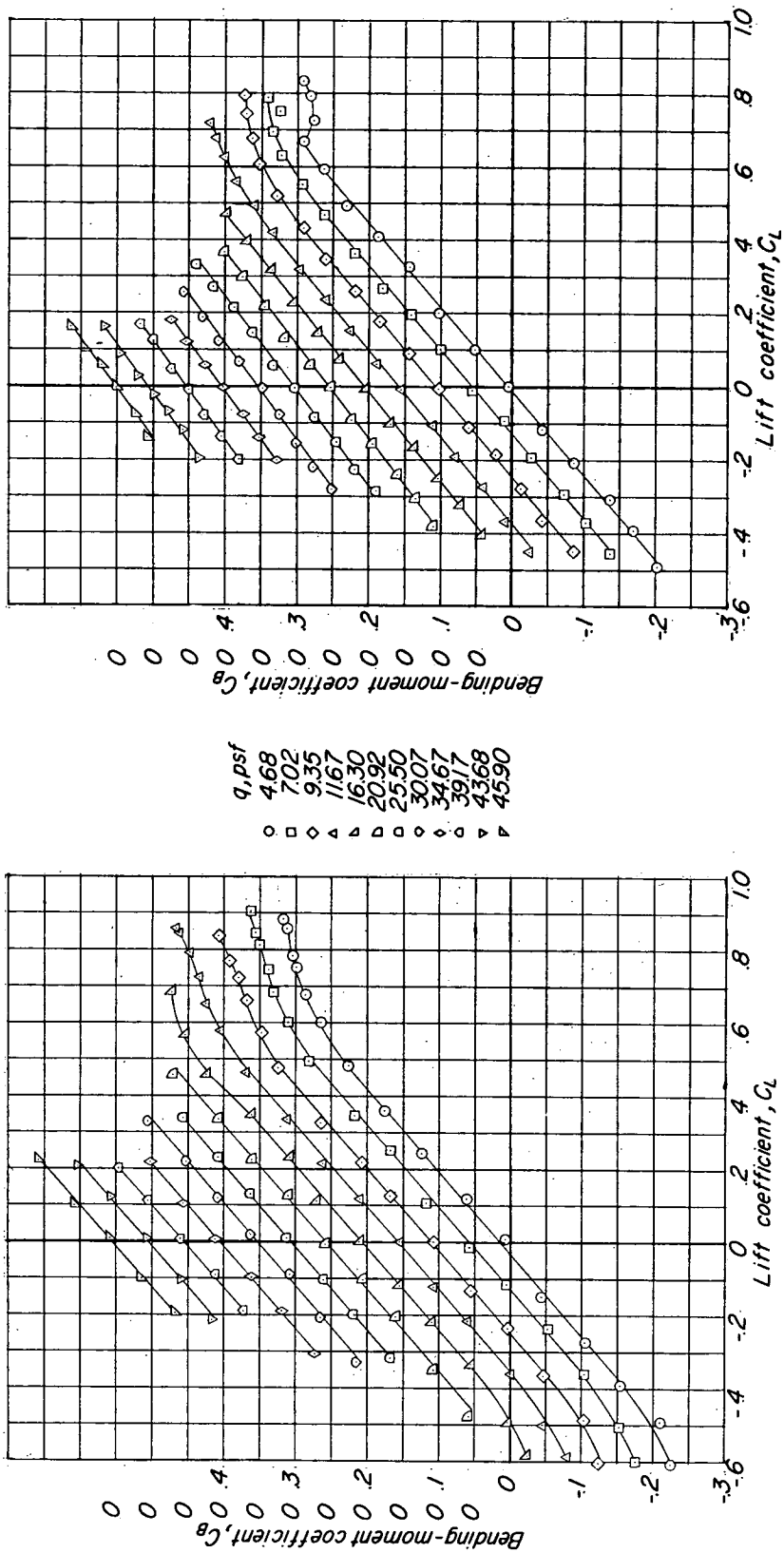

(a) Λ_R wing.

(b) Λ_F wing.

Figure 10.- Variation of bending-moment coefficients with lift coefficient for various dynamic pressures.

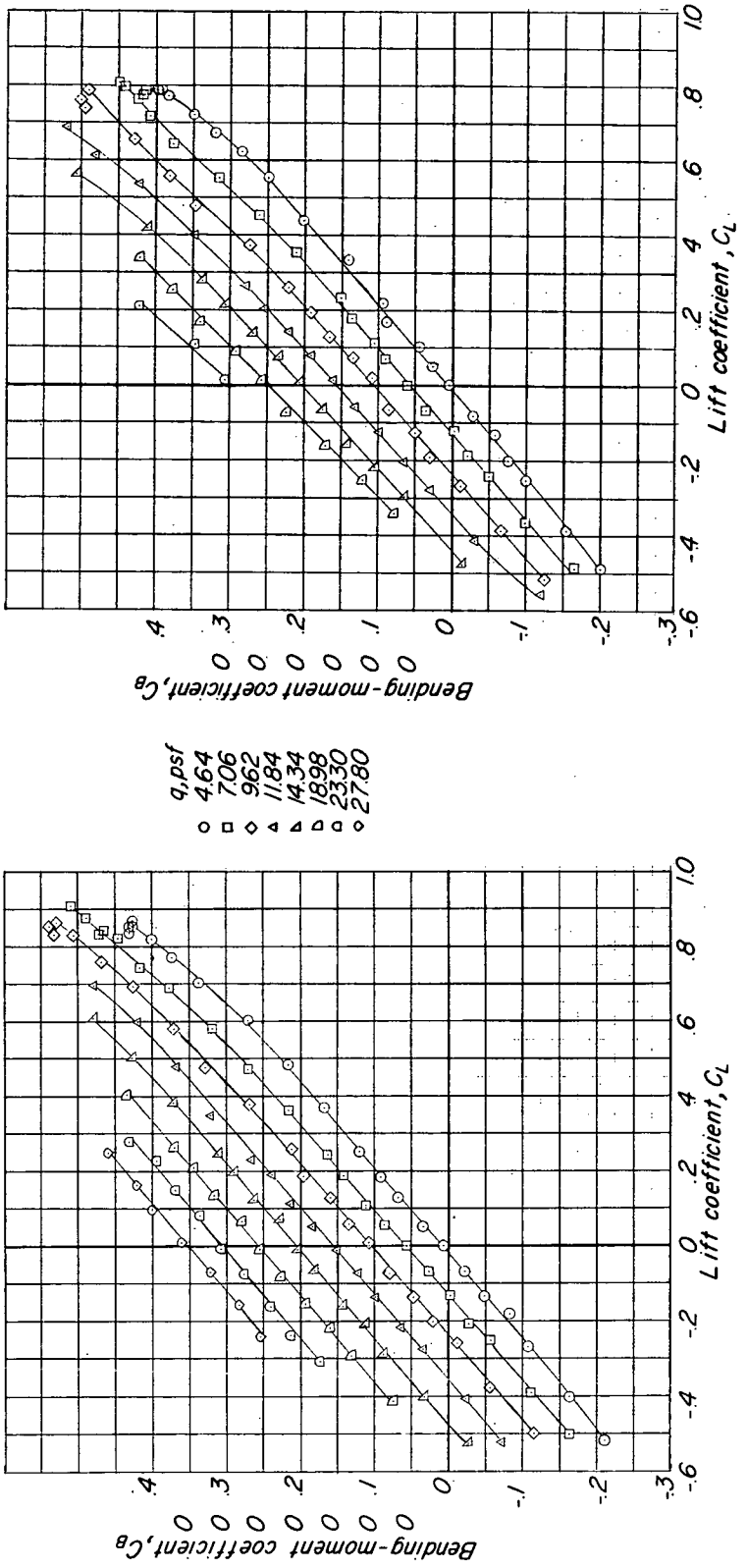

(c) M wing.

(d) W wing.

Figure 10.- Concluded.

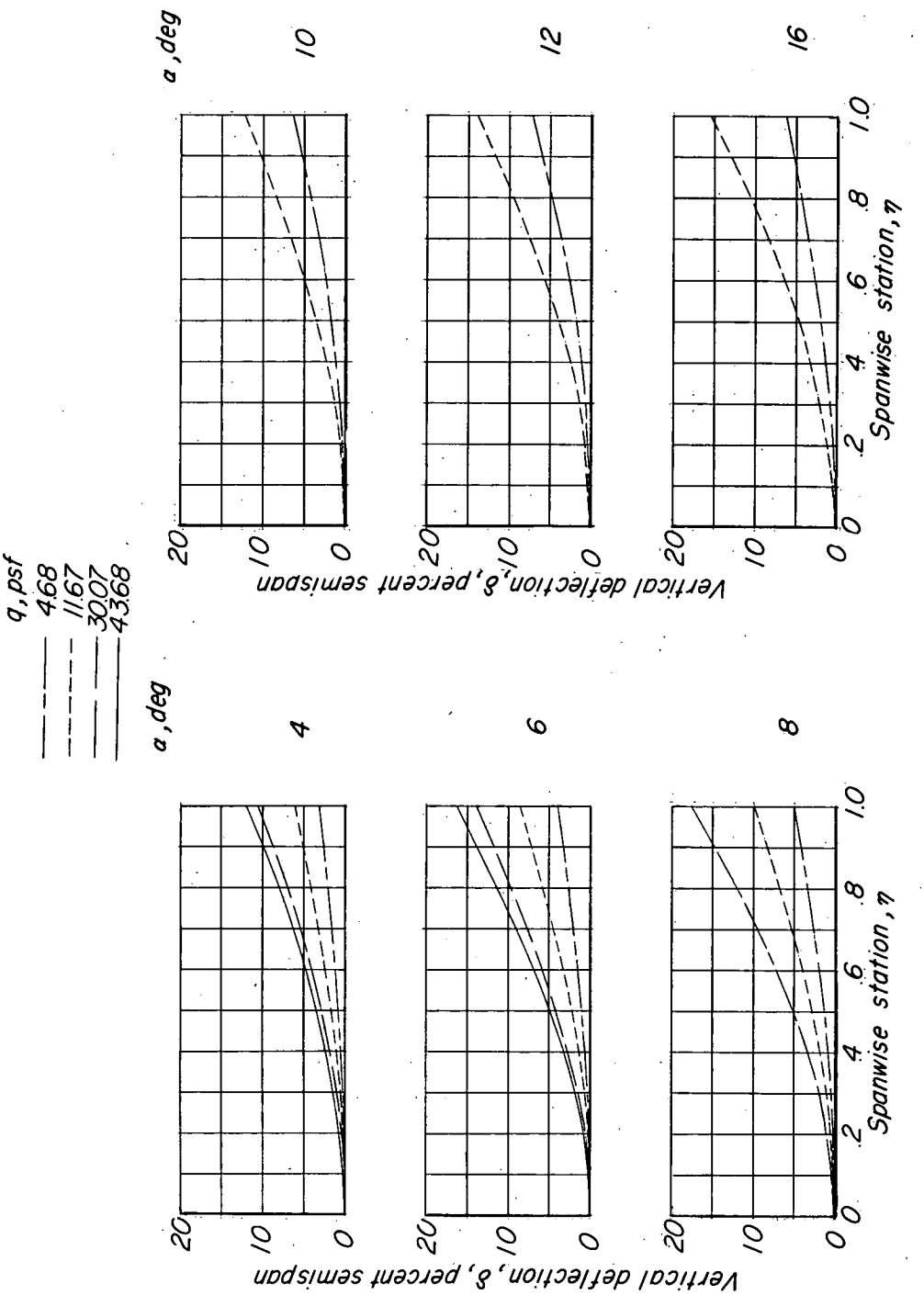

(a) Λ_F wing.

Figure 11.- Spanwise variation of deflection of wing spar for various angles of attack and dynamic pressures.

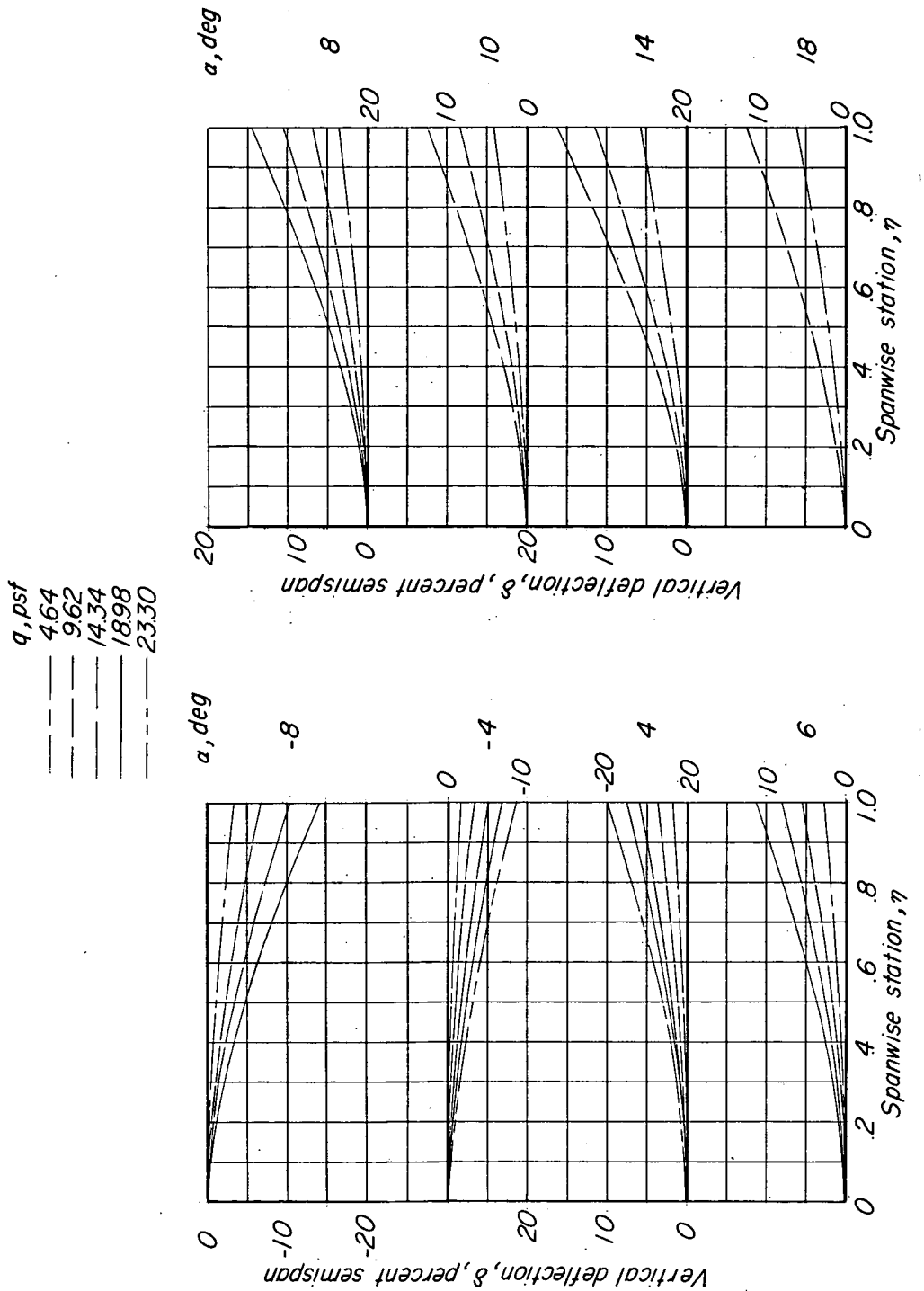

(b) M wing.

Figure 11.- Continued.

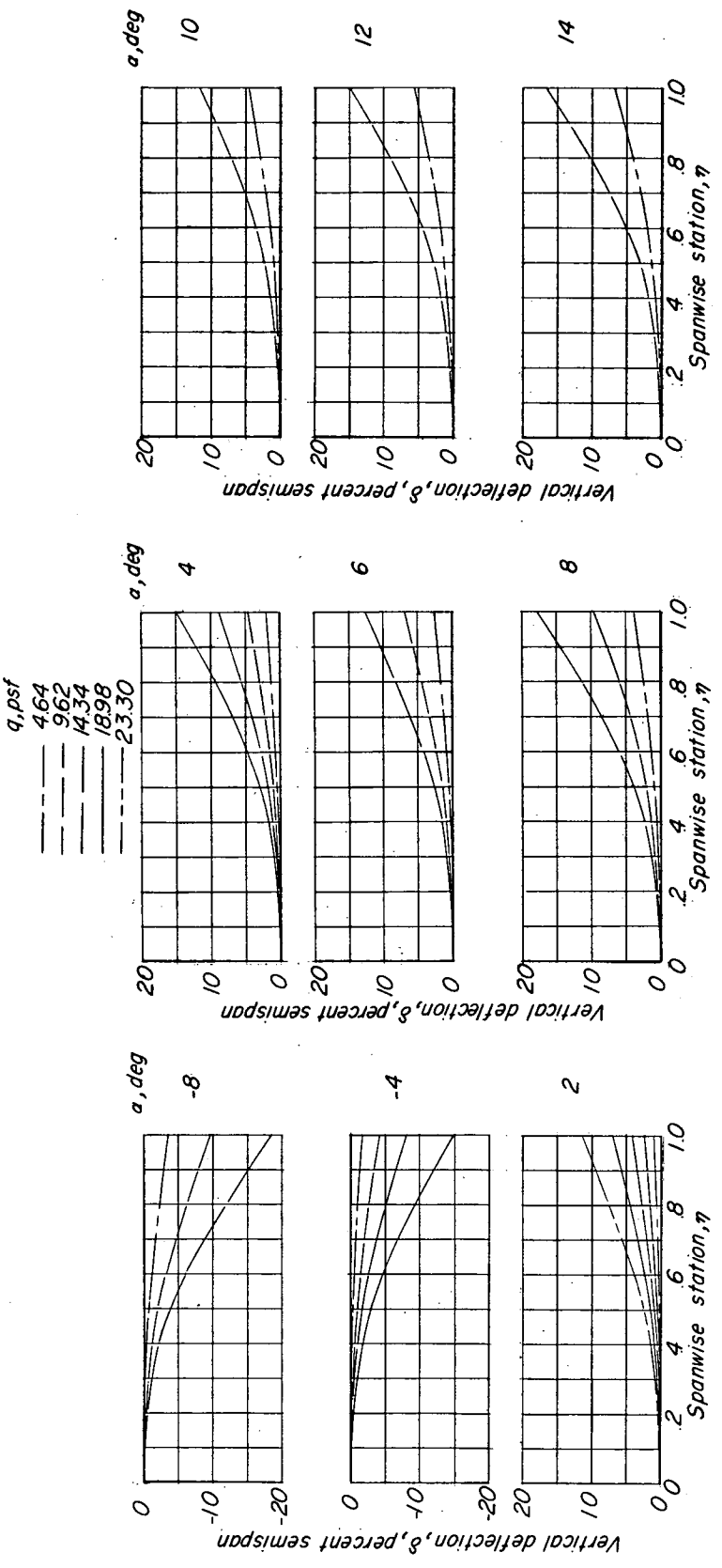

(c) W wing.

Figure 11.- Concluded.

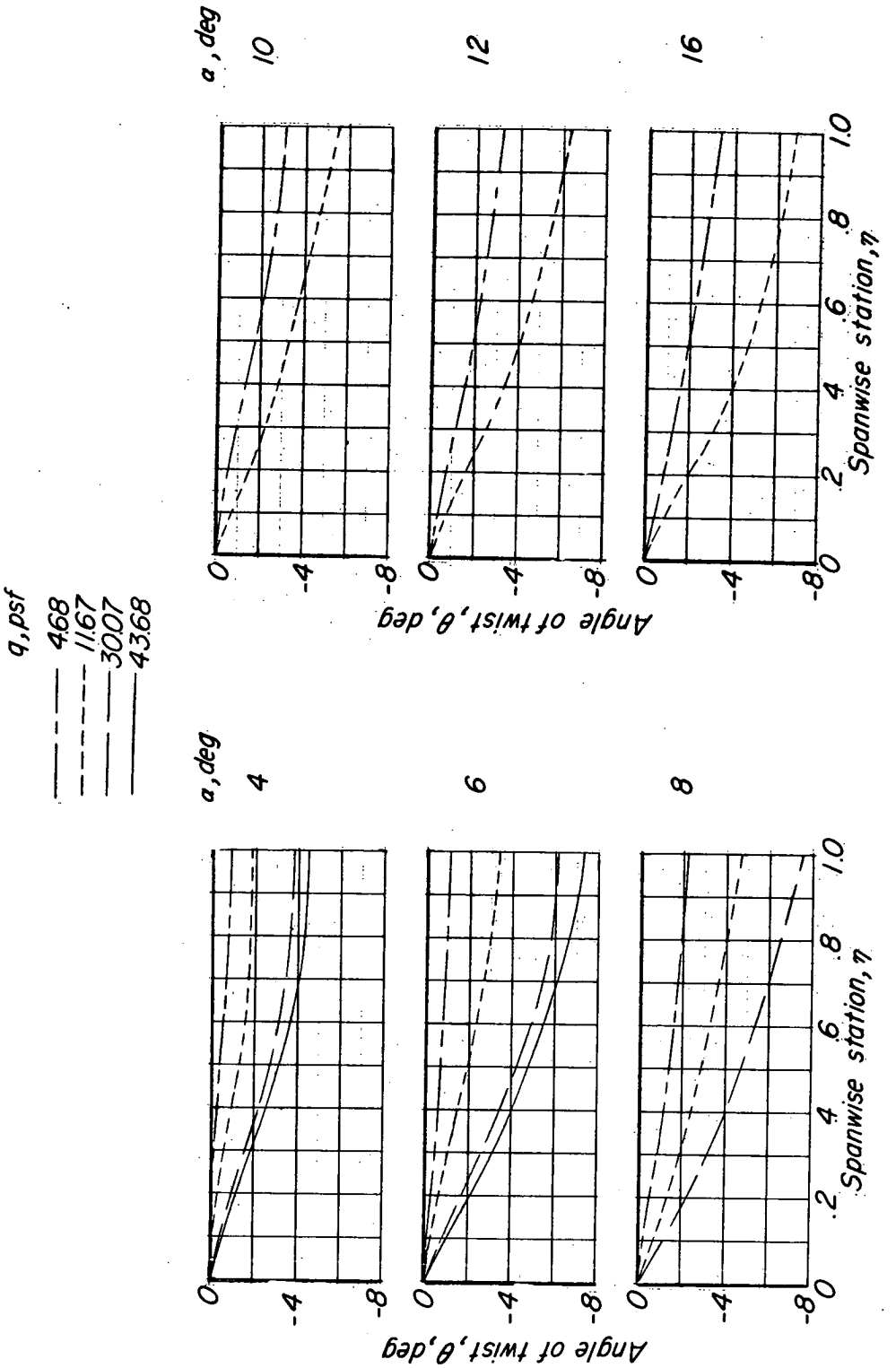

(a) Λ_F wing.

Figure 12.- Spanwise variation of angle of twist, measured in streamwise direction, for various angles of attack and dynamic pressures.

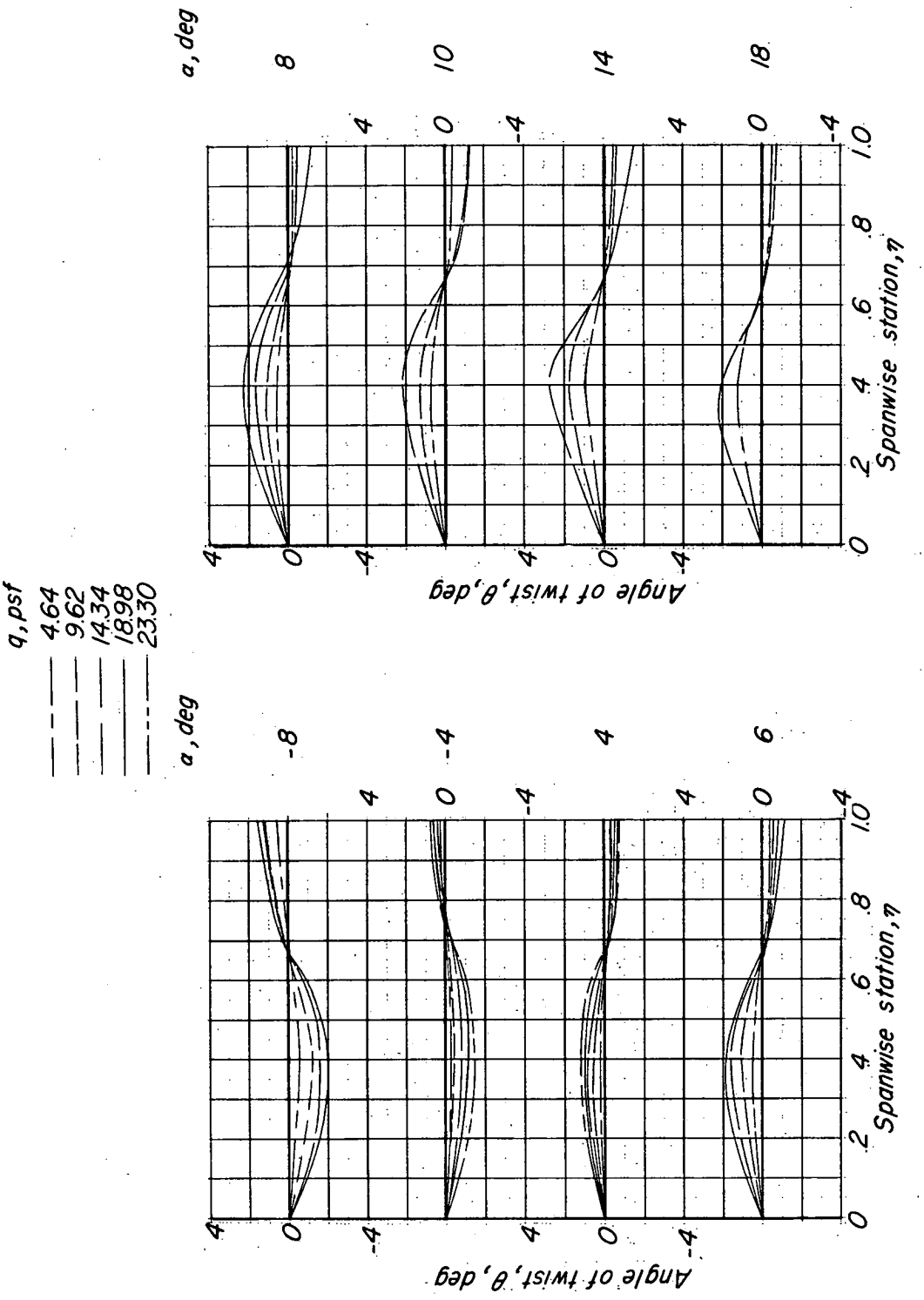

(b) M wing.

Figure 12.- Continued.

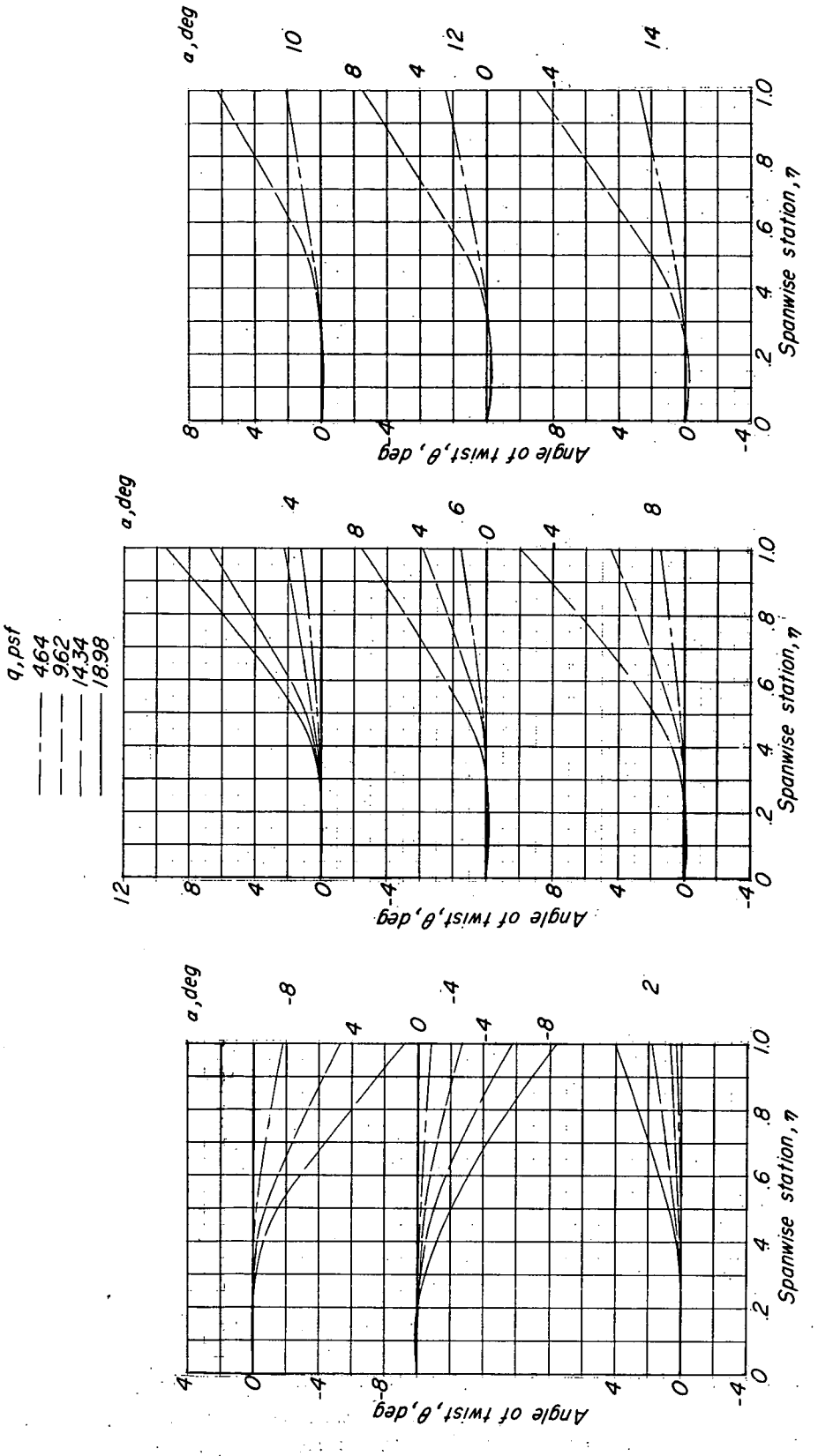

(c) W wing.

Figure 12.- Concluded.

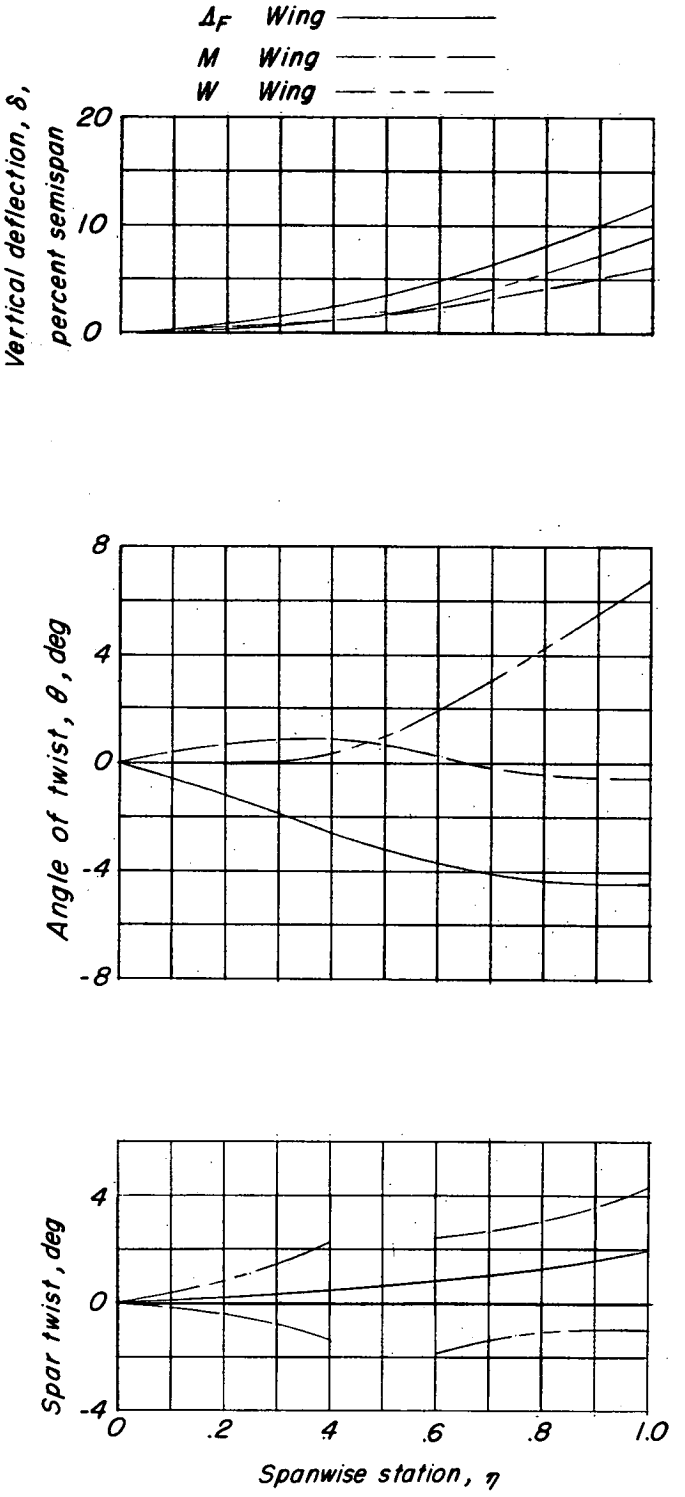

Figure 13.- Spanwise variation of wing vertical bending, wing twist in the streamwise direction, and spar twist, measured in a plane normal to the spar axes, of the Λ_F, M, and W wings at a C_{Lq} of 4.

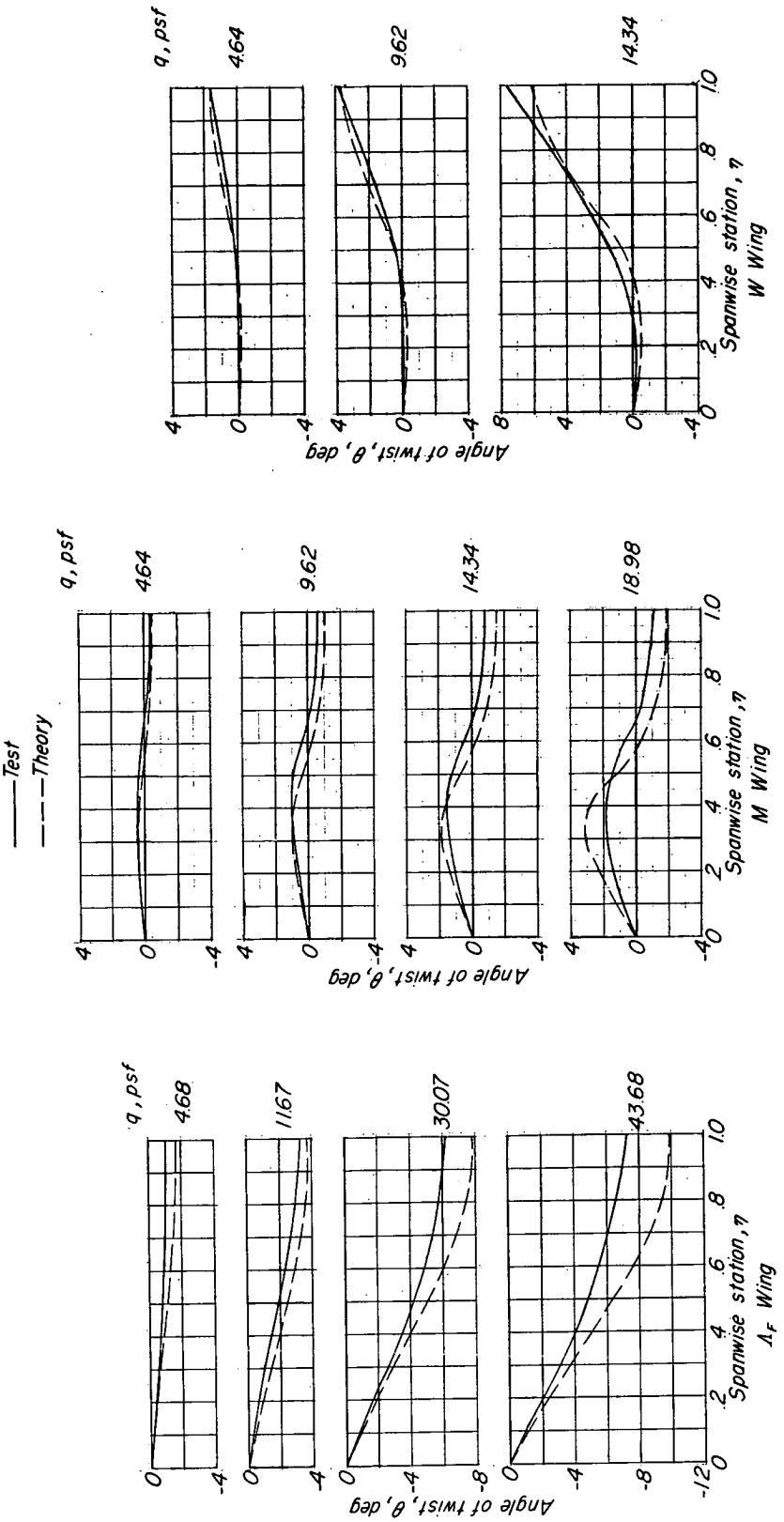

Figure 14.- Comparison of spanwise variation of twist from test and theory (ref. 7) for the Λ_F, M, and W wings at an angle of attack of 6°.

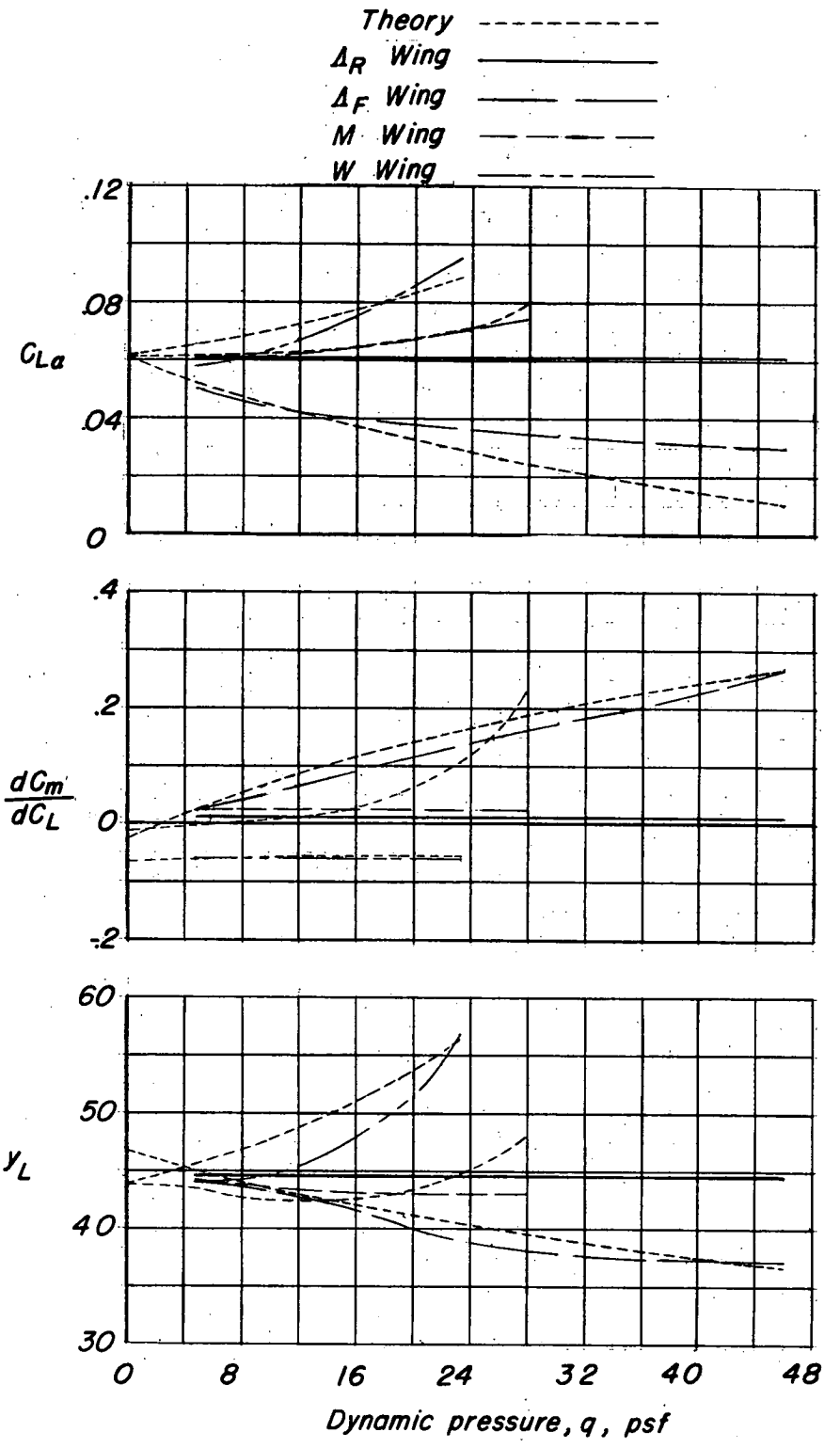

Figure 15.- Summary of the aerodynamic characteristics of the Λ_R, Λ_F, M, and W plan-form wings.

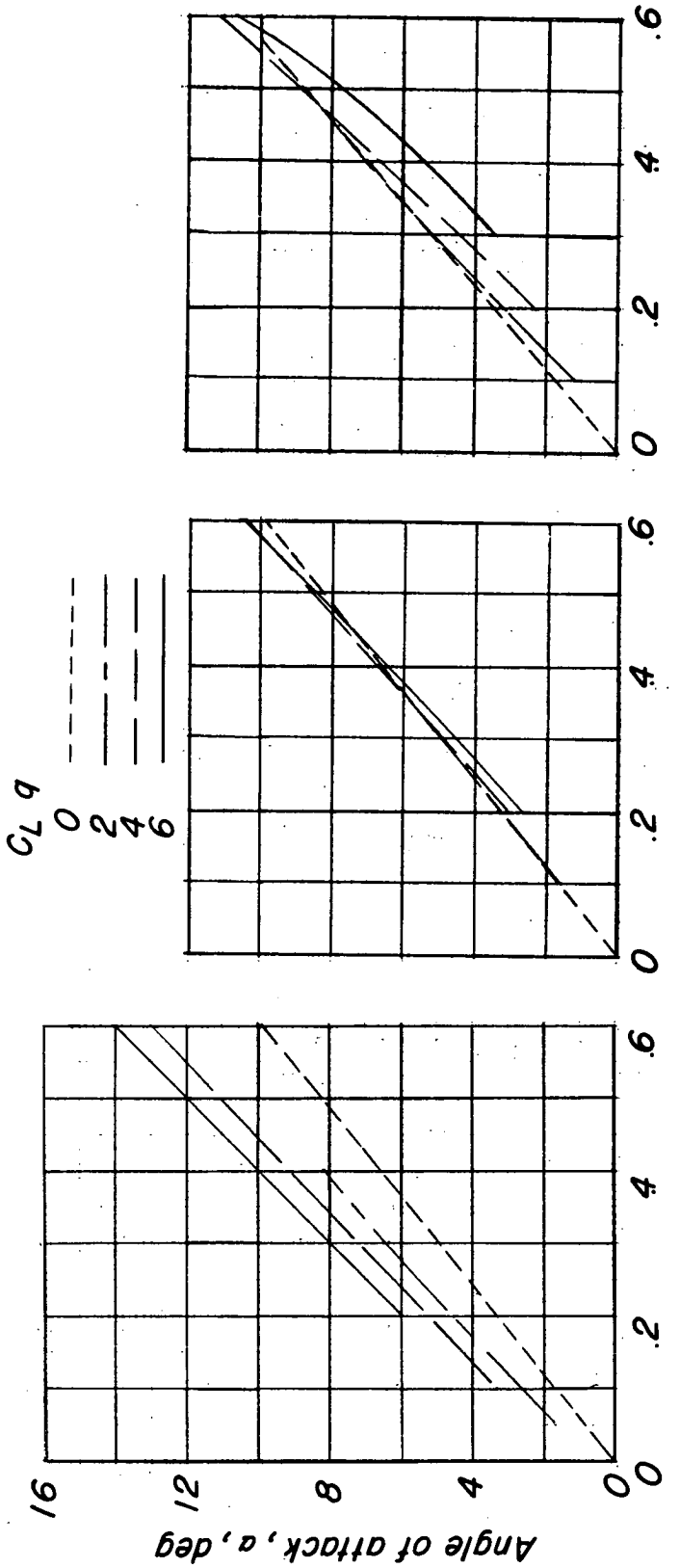

Figure 16.- Variation of angle of attack with lift coefficient at various constant wing loadings.

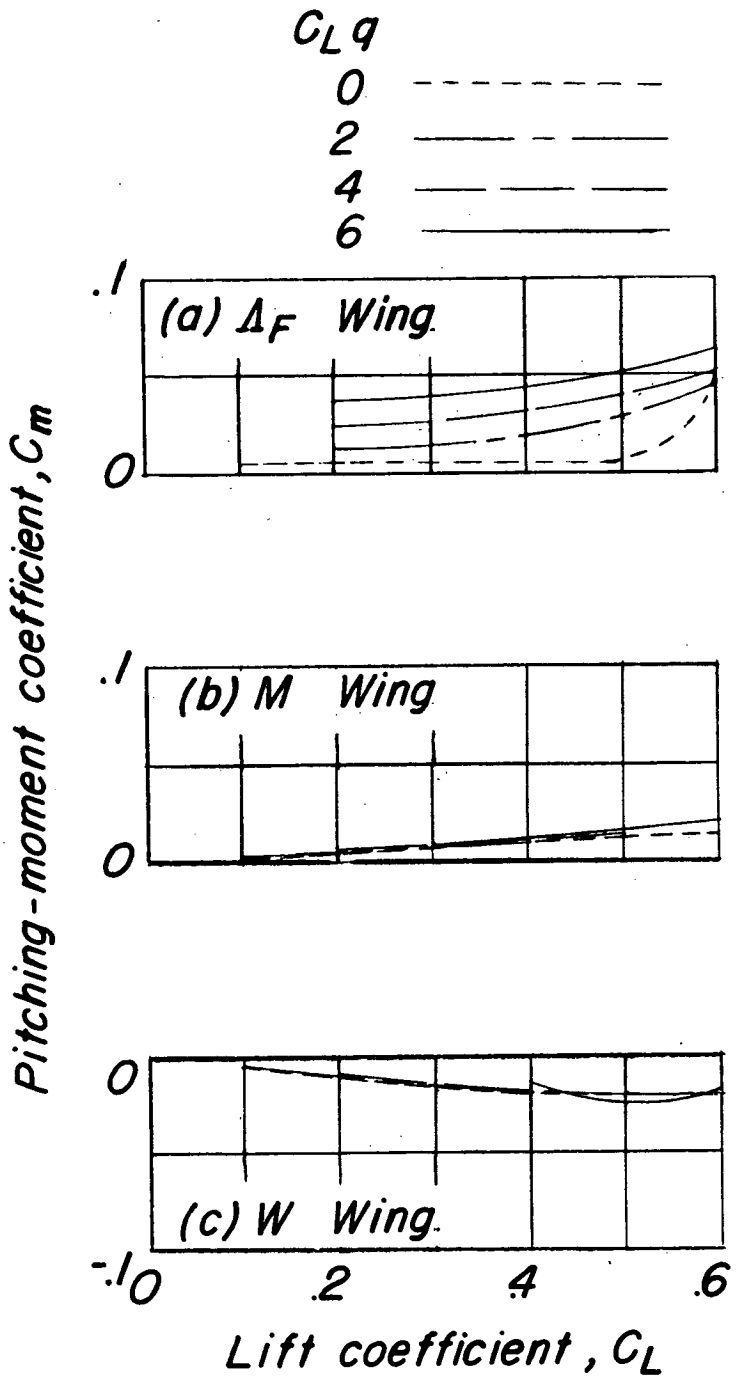

Figure 17.- Variation of pitching-moment coefficient with lift coefficient at various constant wing loadings.

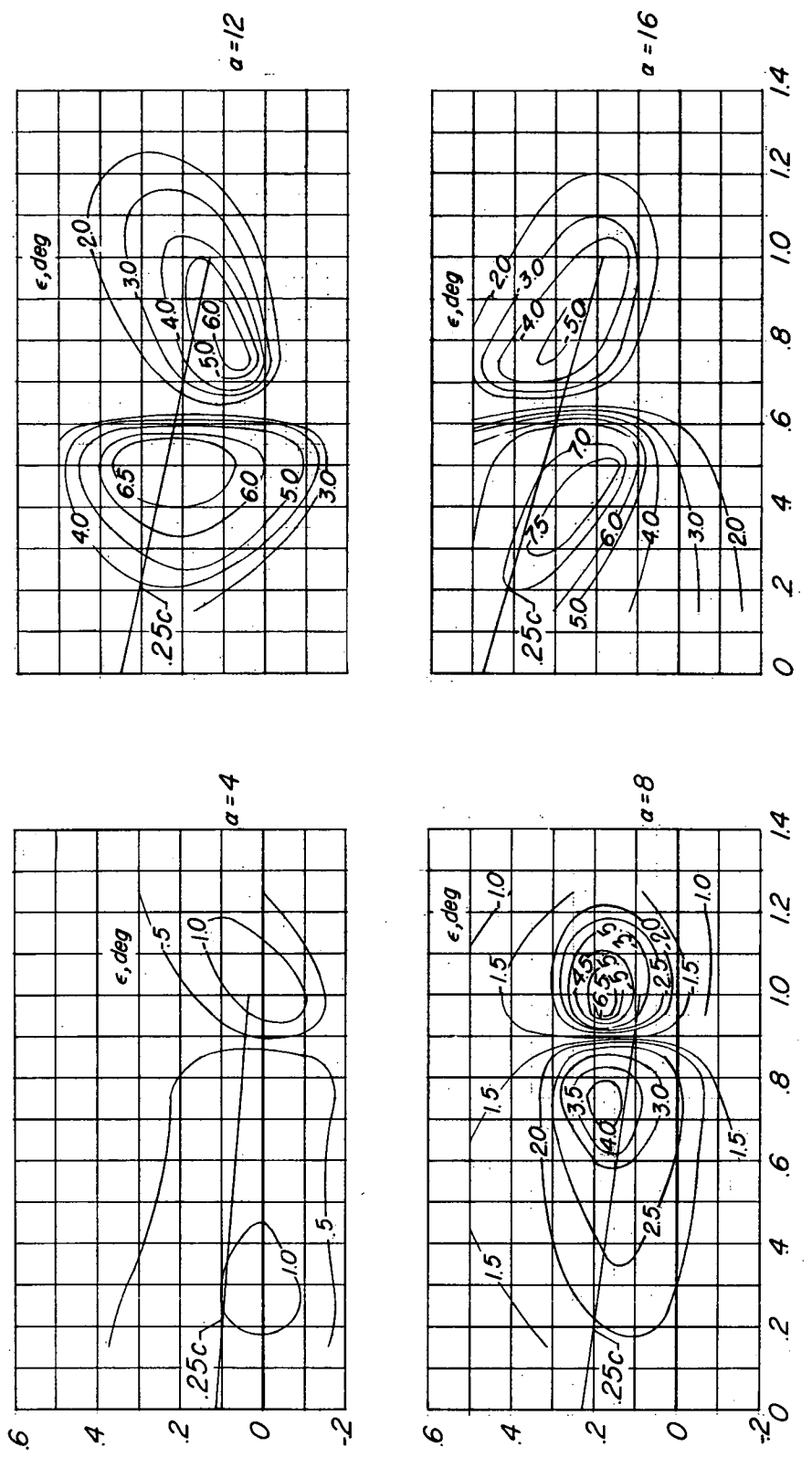

(a) Λ_R wing; q = 18.60 psf.

Figure 18.- Downwash-angle contours in a vertical plane 1.22b/2 behind 0.25 mean aerodynamic chord. (Wing quarter chord as indicated is projection on vertical plane.)

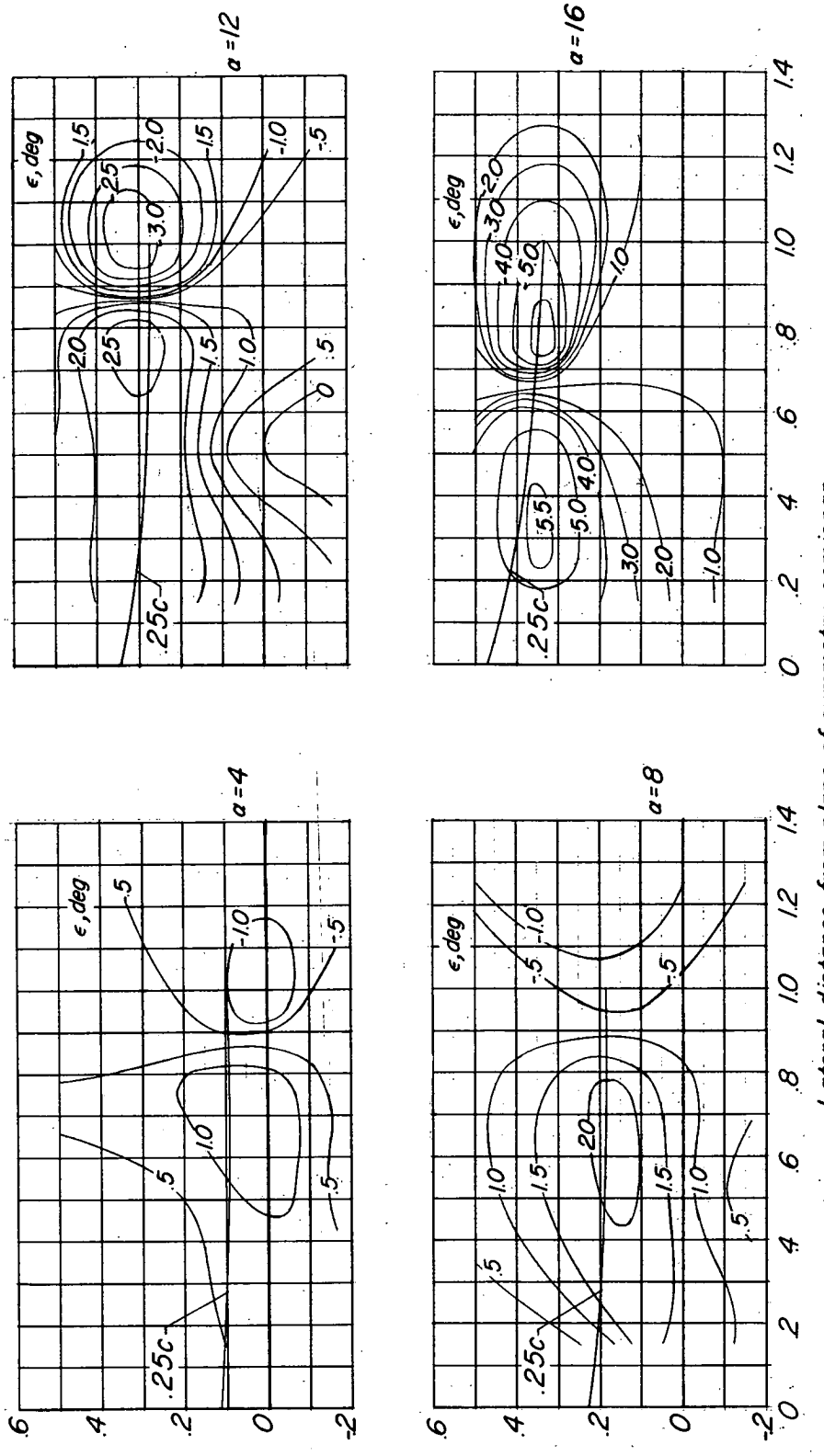

(b) Λ_F wing; q = 11.67 psf.

Figure 18.- Continued.

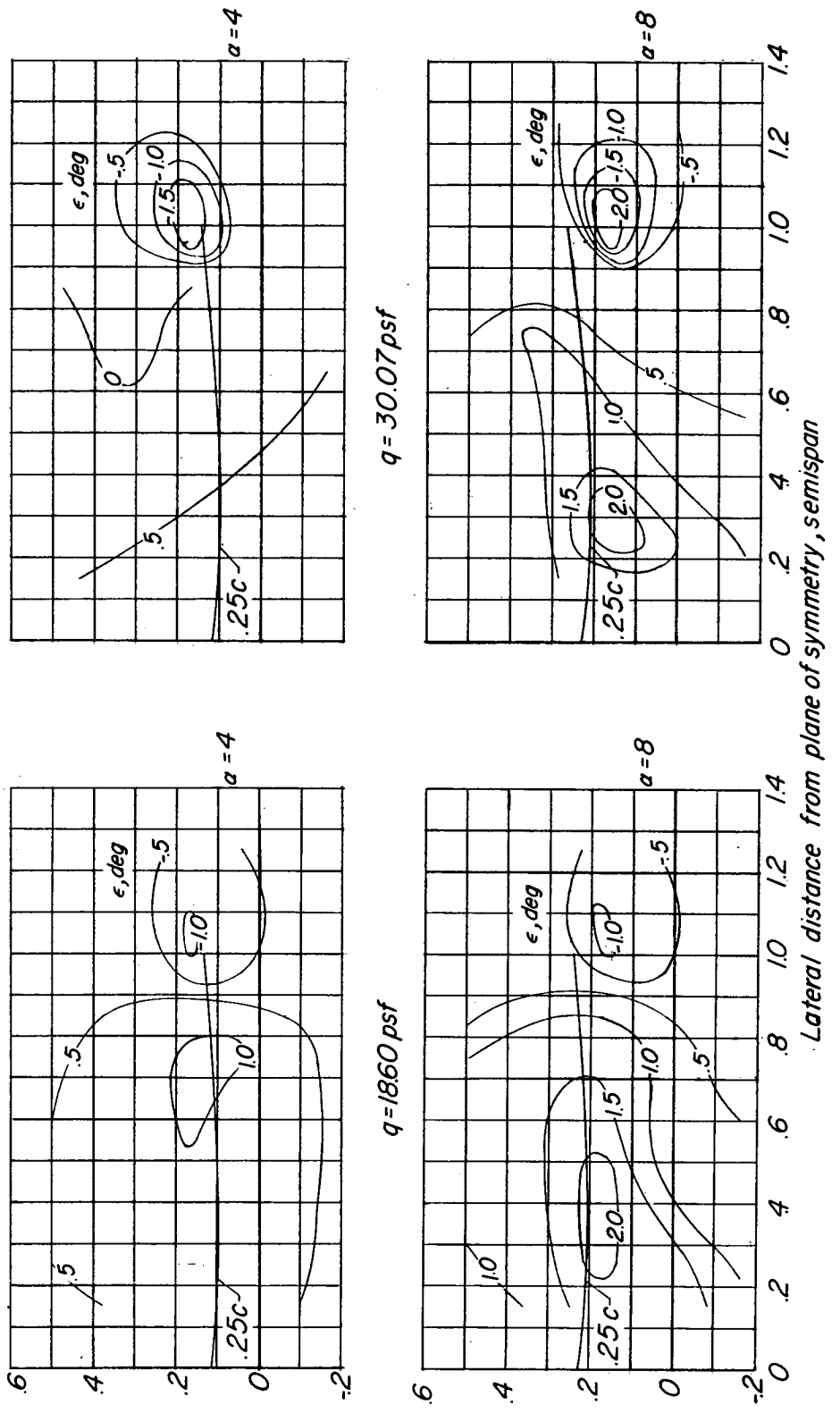

(b) Concluded.

Figure 18.- Continued.

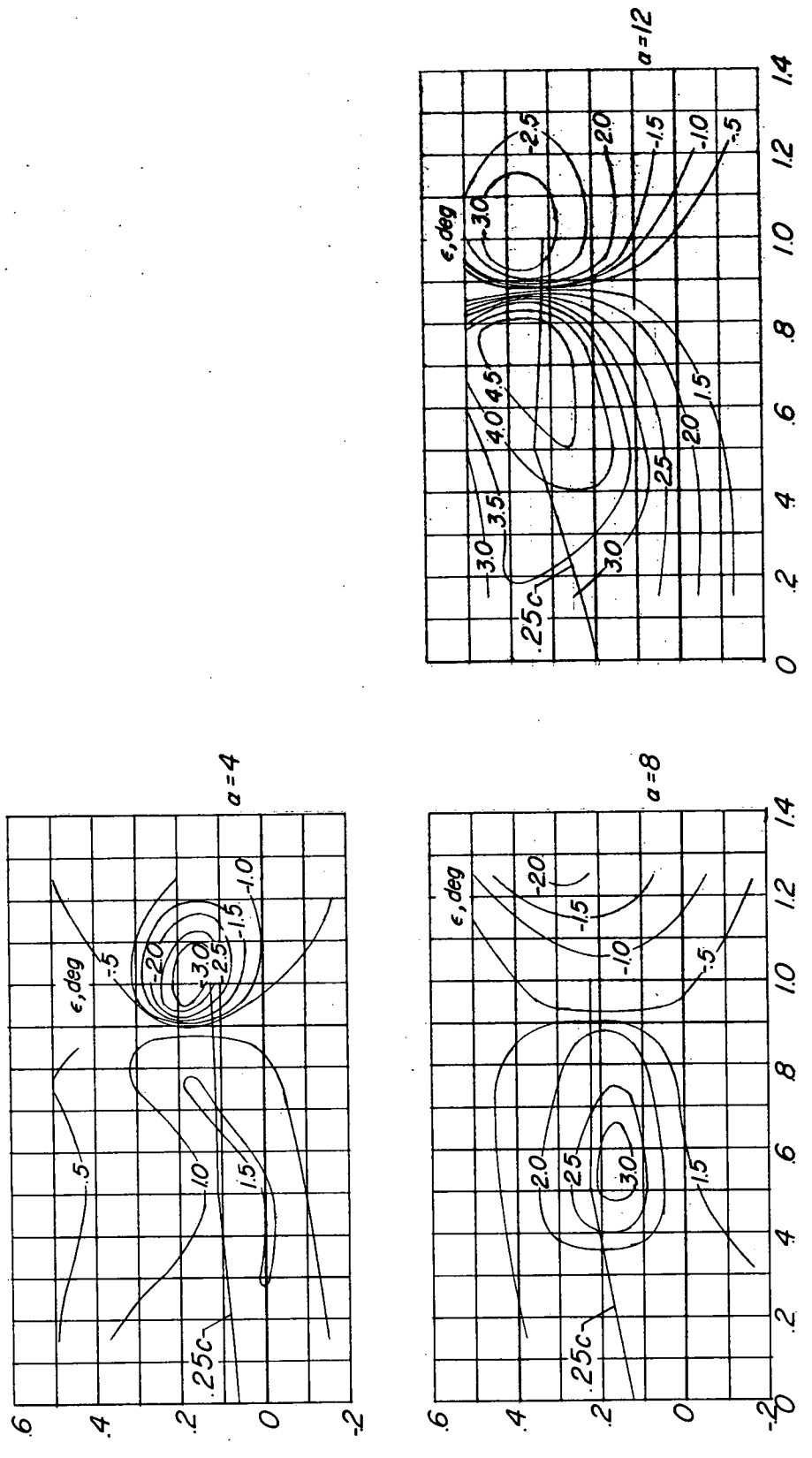

(c) M wing; q = 11.67 psf.

Figure 18.- Continued.

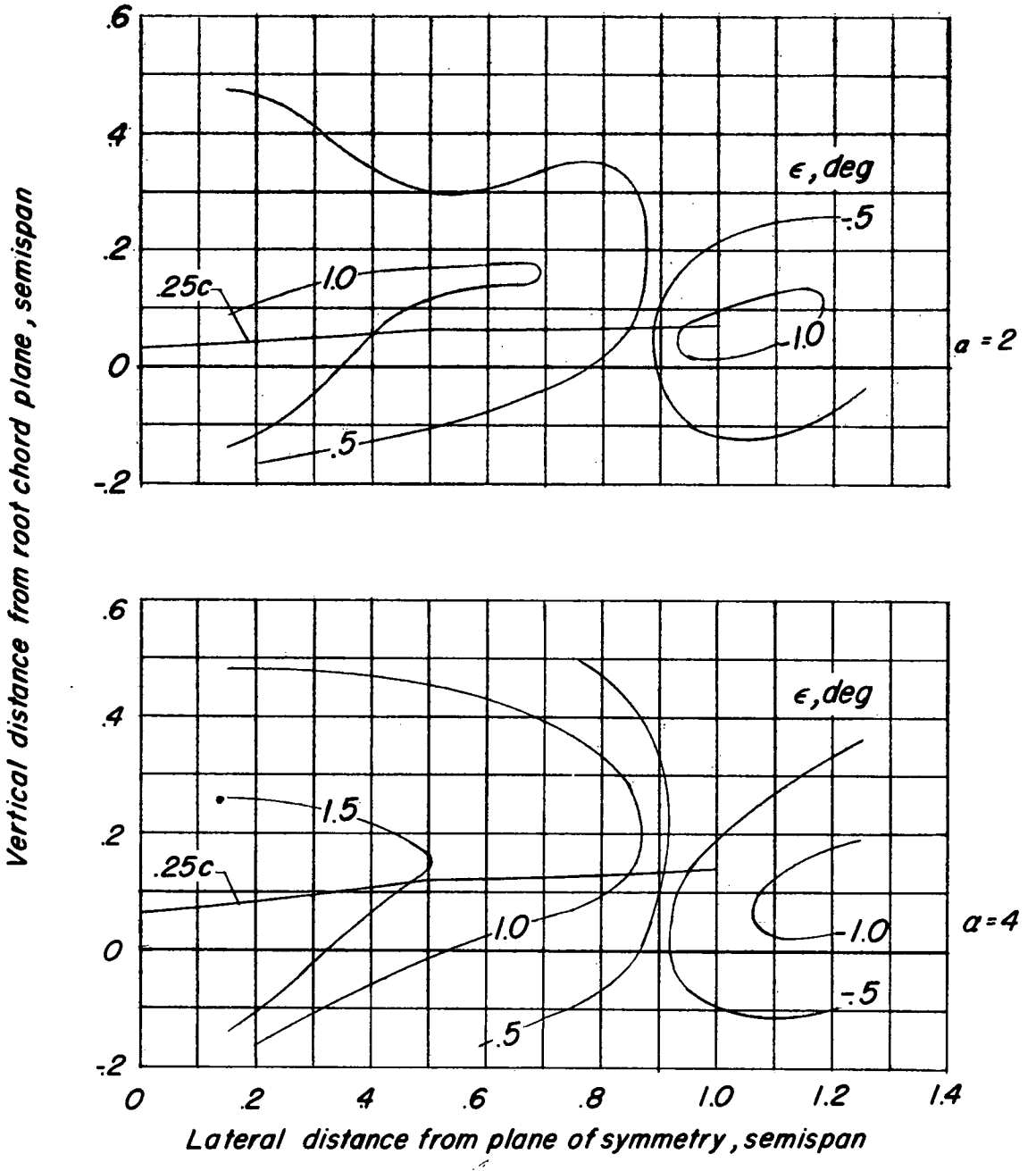

(d) M wing; q = 18.98 psf.

Figure 18.- Concluded.

NACA-Langley - 12-14-53 - 325